LITHOS 456–457 (2023) 107286

Contents lists available at ScienceDirect

LITHOS

journal homepage: www.elsevier.com/locate/lithos

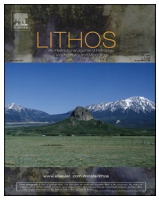

Timescales and mechanisms of felsic lower continental crust formation: Insights from U-Pb geochronology of detrital zircon (Malenco Unit, eastern Central Alps)

Tanya A. Ewing [a,*], Daniela Rubatto [a,b], Kim Lemke [a,b], Jörg Hermann [a]

[a] Institute of Geological Sciences, University of Bern, Baltzerstrasse 3, 3012 Bern, Switzerland
[b] Institut des Sciences de la Terre, University of Lausanne, 1015 Lausanne, Switzerland

ARTICLE INFO

Keywords:
Zircon
U-Pb geochronology
Maximum depositional age
Granulite
Crustal formation
Malenco unit

ABSTRACT

Burial of supracrustal sedimentary material is one of the processes that contribute to the formation of the lower continental crust. We investigate the rate of this process in Permian lower continental crust from the Malenco Unit (eastern Central Alps) by constraining the age of protolith deposition and subsequent high-grade metamorphism of felsic, garnet-rich granulites. Detrital zircon cores, many of which are small (<50 μm), were dated by SIMS and yield concordant dates ranging from 387 ± 21 Ma (2σ) to 2380 ± 16 Ma, with the vast majority of the dates falling in the range 450–1000 Ma. For the seven cores in each sample that gave the youngest concordant dates, replicate analyses were carried out. None of these cores had all measured U-Pb dates agree within error, indicating significant disturbance by the Permian granulite facies metamorphism. A $^{206}Pb/^{238}U$ age of 424 ± 6 Ma for a core with two overlapping replicate analyses is the best available constraint on the maximum depositional age of the sedimentary protolith. This maximum depositional age also coincides with the first significant population in the probability density plot of detrital core dates, which is a double peak at ~425 Ma and ~450 Ma.

Zircon detrital cores are separated from metamorphic overgrowths by a small seam of zircon that is riddled with tiny inclusions of quartz, biotite and muscovite. The first generation of metamorphic zircon rims has a $^{206}Pb/^{238}U$ age of 272.9 ± 2.8 Ma, displays steep heavy rare earth element (HREE) patterns and a moderate negative Eu-anomaly, and returns Ti-in-zircon temperatures of 740–780 °C. The second generation of metamorphic rims has a $^{206}Pb/^{238}U$ age of 263.8 ± 2.6 Ma, a flat HREE pattern and a pronounced negative Eu-anomaly, and gave Ti-in-zircon temperatures of 780–810 °C. Collectively these observations indicate that the first zircon rim formed on the prograde path at the onset of partial melting where muscovite was present but the rocks contained little garnet and no K-feldspar. Therefore, the metapelites resided at lower amphibolite facies, subsolidus conditions up until the intrusion of a Permian gabbro, which was emplaced shortly after the formation of the first generation of metamorphic zircon and caused heating to granulite facies conditions and widespread partial melting. There is no record of high-pressure metamorphism preceding granulite facies conditions, indicating that felsic lower crust in the Malenco unit was not formed by relamination.

The Malenco unit was situated at the north-eastern active margin of Gondwana 420 Ma ago. Subduction-related accretion of sediments at lower crustal levels shortly after their deposition could explain the formation of this felsic lower crust that resided at subsolidus conditions for up to 100 My prior to Permian extension, gabbro intrusion and granulite facies metamorphism.

1. Introduction

The composition of the lower continental crust is relevant to understanding the processes by which the Earth is differentiated into crust and mantle, and for models of crustal growth through time (Cawood et al., 2013; Rudnick, 2018). However, accurately constraining the geochemical composition of the lower continental crust has proved challenging, owing to the inability to sample it directly and

* Corresponding author.
E-mail address: tanya.ewing@gmail.com (T.A. Ewing).

https://doi.org/10.1016/j.lithos.2023.107286
Received 5 April 2023; Received in revised form 2 July 2023; Accepted 7 July 2023
Available online 13 July 2023

uncertainties about the representativeness of the available indirect samples of this reservoir (e.g. Hacker et al., 2011; Rudnick and Gao, 2003).

The lower continental crust has traditionally been regarded as dominantly mafic, based on seismic velocity data and suites of lower crustal xenoliths (e.g. Rudnick and Gao, 2003), although important quantities of felsic metasedimentary granulites are also observed in some lower crustal exposures such as the Ivrea Zone (e.g. Redler et al., 2012). The predominantly mafic view of the lower crust has been challenged by the 'relamination model', which proposes that much of the lower continental crust may be felsic and metasedimentary, and produced by the relamination of the felsic part of subducted continental-derived material to the base of the crust through a variety of subduction zone processes (Hacker et al., 2011). The formation of felsic lower crust by relamination would result in its sedimentary protoliths being rapidly taken to high pressure conditions on their way to becoming lower crust, with the pressure peak preceding, and significantly exceeding, the lower crustal pressures at which they eventually settle. This represents a distinctly different prograde evolution from other formation models that could be envisaged for felsic lower crust, such as the burial of accretionary wedge sediments to lower crustal depths during subduction and accretion (Ducea et al., 2009). Such a process would be characterised by steadily increasing, but overall lower pressures with the final lower crustal pressures representing the baric peak. Recently, Wyatt et al. (2022) proposed a model for the formation of the felsic lower crust in the Ivrea Zone (northern Italy) that involves rapid burial and accretion of sediments shortly after their deposition, in which the metasediments experience a pressure peak that predates the granulite facies overprint associated with the emplacement of a Permian mafic complex.

In this contribution, we investigate the timescales and mechanisms of formation of felsic lower continental crust in a well-documented exposure of lower crustal metasedimentary granulites from Val Malenco, eastern Central Alps (Italy). The Val Malenco granulites represent one of several fragments of preserved Permian lower continental crust with a significant metasedimentary component that are now exposed in the European Alps (Müntener and Hermann, 1996). These lower crustal fragments have been widely studied for their Permian high-grade metamorphic history (Müntener et al., 2000) and subsequent evolution during Jurassic rifting related to opening of the Tethys ocean (Müntener and Hermann, 2001). Thus far, little attention has been paid to the pre-Permian history of these lower crustal relics, including how this felsic lower crust was originally formed. The Malenco unit is ideally suited to study the generation of felsic lower crust, as it preserves metasedimentary granulites that are directly welded to upper mantle lithologies by a gabbroic intrusion, providing clear evidence that they represented the lowermost continental crust in the Permian (Hermann et al., 1997).

We use U-Pb geochronology of detrital zircon cores to determine a maximum depositional age for the sedimentary protolith of the Malenco felsic granulites. This is coupled with U-Pb dating and trace element analysis of metamorphic zircon domains in the same metapelites, which constrain the timing and conditions of granulite facies metamorphism under lower crustal conditions (previously documented by Hermann and Rubatto, 2003). Together these new age constraints define the maximum time window between deposition of the sedimentary protolith at the Earth's surface, and granulite facies metamorphism under lower crustal conditions, thus constraining the timescales of formation of this felsic lower continental crust. The zircons in our granulites are complex, with detrital cores and multiple generations of metamorphic overgrowths. The complexity of the zircons and the small size of many of the domains demand a tailored analytical approach. We measured U-Pb ages by secondary ion mass spectrometry (SIMS), the high spatial resolution of which allows analysis of small cores and metamorphic overgrowths, and also permits replicate analyses of key detrital cores to screen for dates disturbed by high-grade metamorphism and thus ensure accurate determination of maximum depositional age. Our results demonstrate that this type of approach is essential in high-grade samples to avoid obtaining erroneous maximum depositional ages. We complement zircon geochronology and trace element data with petrography, which provides further constraints on the prograde metamorphic evolution of the metasedimentary granulites, in order to explore the validity of different models for formation of this lower continental crust.

2. Geological setting

The Malenco unit (Val Malenco, northern Italy) is part of the eastern Central Alps and preserves a fossil section through the Permian lower continental crust and uppermost mantle (Hermann et al., 1997; Hermann and Rubatto, 2003; Müntener et al., 2000; Müntener and Hermann, 1996) (Fig. 1). The Permian Braccia gabbro is intrusive into upper mantle units and lower crustal metasedimentary rocks, which collectively preserve a continuous sequence of subcontinental mantle and lowermost continental crust of Permian age (Hermann et al., 1997; Müntener and Hermann, 1996). Subcontinental mantle rocks of the Malenco unit are dominantly spinel peridotites with subordinate dunites and pyroxenites (Müntener and Hermann, 1996), while the lower continental crustal rocks are mainly represented by metapelites and intercalated metacarbonates (Hermann and Rubatto, 2003). The Braccia gabbro complex is dominated by gabbro-norites and was produced by decompression melting of asthenospheric mantle during Permian lithospheric extension, and emplaced at the base of the continental crust, welding the lower crustal metasedimentary sequence to the underlying lithospheric mantle (Hermann et al., 1997, 2001). Emplacement of the gabbroic complex induced granulite facies metamorphism and extensive partial melting of the Malenco metapelites, with a granulite facies paragenesis characterised by garnet, plagioclase, quartz, ilmenite, minor biotite, K-feldspar and rare kyanite (Hermann et al., 1997; Hermann and Rubatto, 2003; Müntener et al., 2000). Phase relations and mineral compositions indicate peak pressures of 1 GPa and temperatures of 800–850 °C for the granulite facies metamorphism (Hermann et al., 1997; Hermann and Rubatto, 2003; Müntener et al., 2000). Peak metamorphic temperatures are inferred to have been reached at the time of emplacement of a small granitic body, which is dated at 278.4 ± 2.6 Ma (Hansmann et al., 2001; Hermann and Rubatto, 2003). Zircon and monazite U-Pb geochronology of a granulite facies metasediment testify to a protracted (ca. 20 Myr) period of granulite facies conditions (Hermann and Rubatto, 2003). The youngest concordant detrital zircon core age (determined on a single metapelite sample) was 520 ± 11 Ma, indicating a post-Pan African maximum depositional age for the Malenco metasediments (Hermann and Rubatto, 2003). However, the main aim of that study was to constrain the metamorphic evolution of the granulites, and only a few detrital cores were dated. Detailed study of the detrital core age spectra and maximum depositional age is lacking.

The previous study of a single Malenco metapelite sample identified three generations of metamorphic zircon rims, each of which had distinct age, geochemistry and cathodoluminescence characteristics (Hermann and Rubatto, 2003). Trace element geochemistry and mineral inclusions were used to link these ages to different parts of the Permian metamorphic evolution. A first generation of metamorphic zircon formed at 281 ± 2 Ma during fluid-absent partial melting on the prograde path, followed by a second generation at 269 ± 3 Ma produced by cooling of partial melts from the initial thermal peak associated with the gabbro emplacement (Hermann and Rubatto, 2003). The final generation of metamorphic zircon formed at 258 ± 4 Ma and records a second episode of partial melting caused by a reheating driven by the shallow asthenosphere generated by an extensional regime (Hermann and Rubatto, 2003). The age of the first (prograde) generation of metamorphic zircon in the metasedimentary granulite is within error of TIMS U-Pb upper intercept ages for the emplacement of the Braccia gabbro (281 ± 19 Ma) and a small granitic body produced by partial melting of the metapelites (278.4 ± 2.6 Ma) (Hansmann et al., 2001). The geochronology thus supports field, petrographic and petrologic

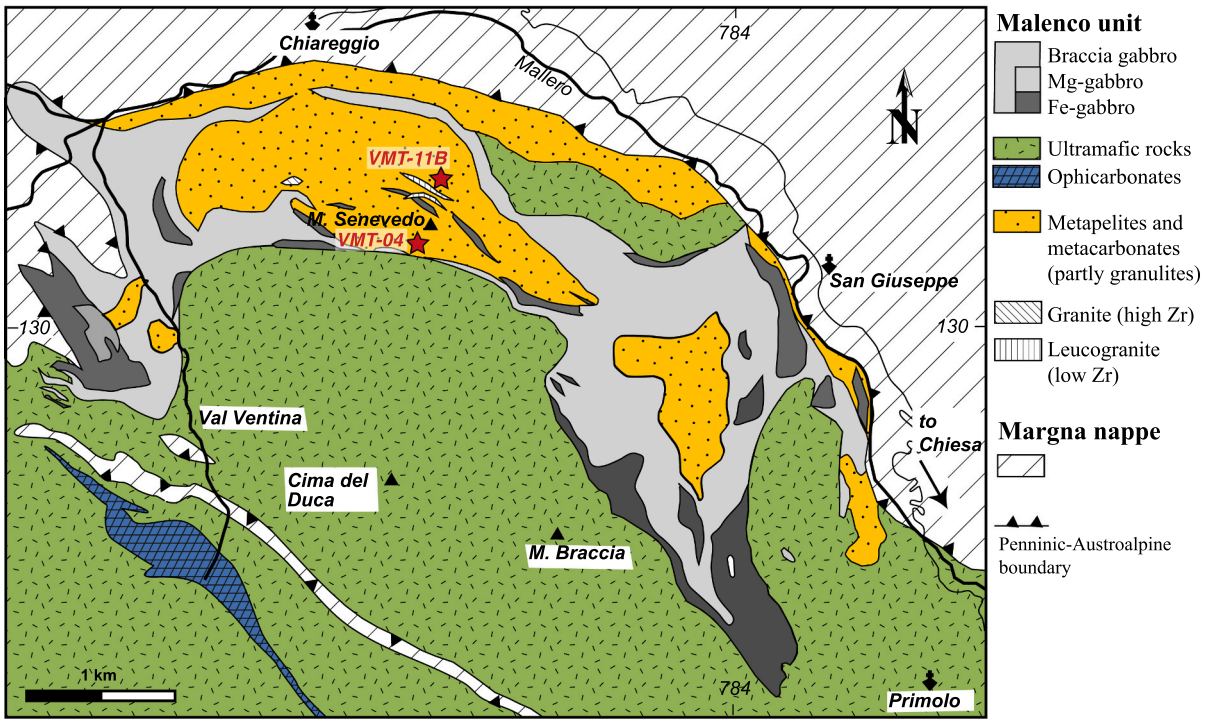

Fig. 1. Geological map of the Val Malenco region, modified after Müntener and Hermann (1996) and Hermann and Rubatto (2003). The sample locations are indicated with red stars. (For interpretation of the references to colour in this figure legend, the reader is referred to the web version of this article.)

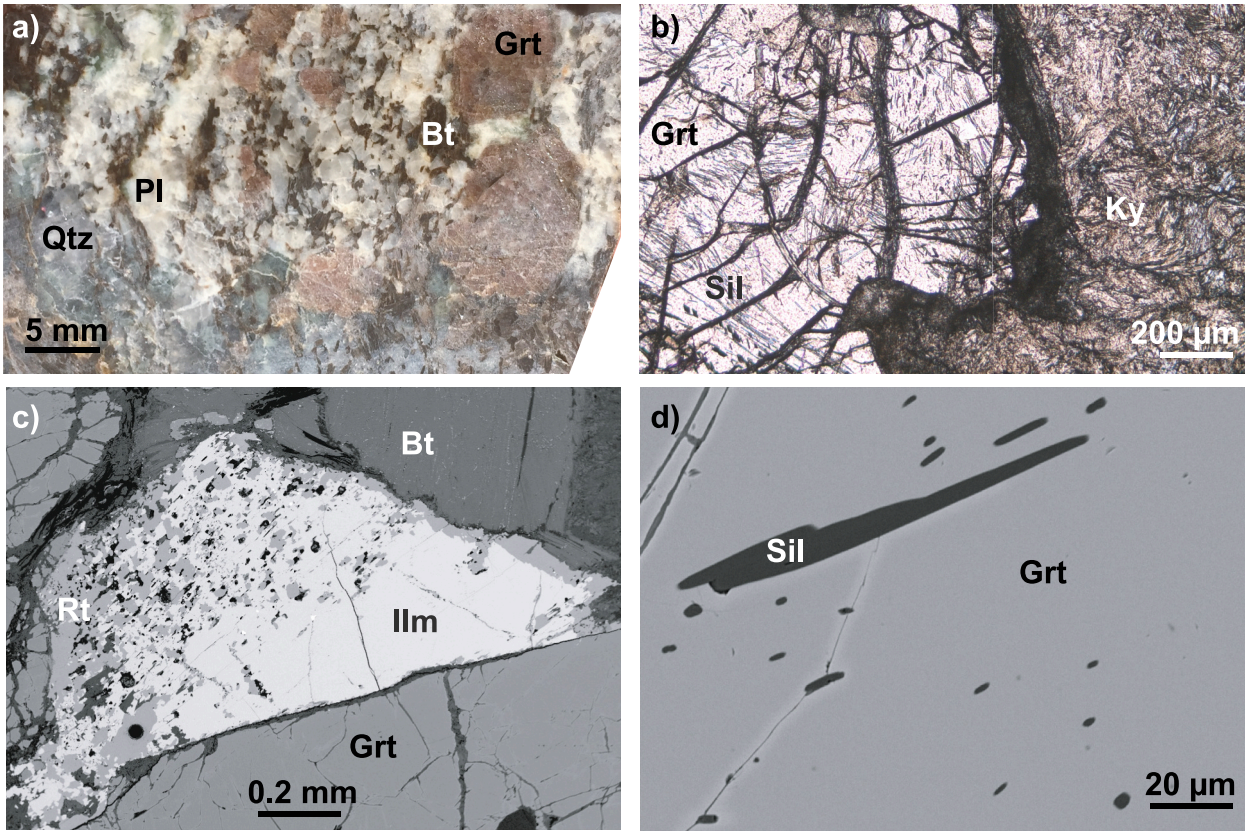

Fig. 2. a) Overview of sample VMT-11B in hand specimen, with large restitic garnet (Grt) and migmatitic texture of plagioclase (Pl), quartz (Qtz) and biotite (Bt). b) Transmitted light image of thin section showing garnet with inclusions of sillimanite (Sil). The granulite facies sillimanite is completely replaced by amphibolite facies kyanite (Ky) in the matrix of the sample. c) Partial replacement of ilmenite (Ilm) by rutile (Rt) seen in BSE. d) BSE image of sillimanite inclusions in garnet.

observations that indicate that the intrusion of the gabbro initiated the granulite facies metamorphism and partial melting of the metapelites (Hermann et al., 1997; Hermann and Rubatto, 2003; Müntener et al., 2000).

The protracted granulite facies conditions were followed by near-isobaric cooling of both metasedimentary and gabbroic lithologies, which remained stable lower crust for ca. 50 Myr (Müntener et al., 2000). In Jurassic times, the Malenco crust–mantle section was exhumed to form part of the ocean–continent transition of the Adriatic margin during continental rifting that culminated in the opening of the Tethys ocean (Hermann et al., 1997; Hermann and Müntener, 1996; Müntener et al., 2000). Exhumation occurred by near-isothermal decompression and was associated with partial hydration of the granulite facies assemblages (Müntener et al., 2000). Subsequently, during the Alpine orogeny, the Malenco unit underwent epidote–amphibolite facies metamorphism as it was incorporated into the Adriatic–European suture zone (Hermann and Rubatto, 2003). Some of the granulites in the inner part of the nappe escaped the pervasive Alpine recrystallisation that occurred at the nappe boundary (Hermann and Müntener, 1996; Hermann and Rubatto, 2003; Müntener and Hermann, 1996).

3. Samples

A suite of granulite facies metasediments was collected from localities on the northern and southern flanks of Monte Senevedo in Val Malenco. Following petrographic analysis, two samples were selected for zircon separation and analysis (Fig. 1).

Sample **VMT-11B** is a granulite facies metasediment that was sampled as a loose block from the bed of a creek on the northern flank of Monte Senevedo, in a gully above and to the west of Alpe Pirolina (GPS co-ordinates 46°18'40 N, 009°48′04 E, 1872 m). Such blocks originate from the inaccessible cliffs of Monte Senevedo above, and represent the freshest, least retrogressed metasedimentary granulites from this unit (Fig. 2). Sample VMT-11B is heterogeneous with garnet-rich domains and plagioclase- and quartz-rich domains typical for a migmatite. The metasediments show little retrogression of the granulite facies paragenesis and garnet displays minimal replacement by retrograde chlorite (Fig. 2a). The sample is dominated by matrix plagioclase that is partly to heavily altered. Minor K-feldspar is present in the leucocratic domains. Quartz is subordinate and occurs concentrated in patches of coarse-grained crystals. Quartz contains abundant rutile exsolution needles, indicating high initial Ti concentrations and therefore high crystallisation temperatures (e.g. Thomas et al., 2010). Garnet occurs as a few very large (centrimetric) crystals. The cores of the garnet host abundant 10–20 μm-sized inclusions containing aggregates of plagioclase, quartz and biotite, as well as minor chlorite and muscovite. These inclusions represent relics of the amphibolite facies assemblage at the onset of garnet growth. Garnet rims occasionally contain inclusions of sillimanite needles as confirmed by Raman spectroscopy (Fig. 2b,d). In the matrix, sillimanite pseudomorphs are replaced by fine-grained kyanite (Fig. 2b). Minor staurolite also occurs in contact with garnet and biotite in these pseudomorphs. Biotite occurs as large flakes, in some cases concentrated in layers, and in many cases is replaced by retrograde chlorite. Ilmenite is present as large grains in the matrix and included in garnet, and is partially replaced by rutile (Fig. 2c), providing evidence for rutile formation during isobaric cooling. Graphite flakes occur included in garnet as well as in the matrix. Retrograde muscovite and chlorite are widespread. The observed sequence of minerals indicates a prograde, amphibolite facies stage, followed by a granulite facies equilibration with partial melting in the sillimanite stability field. Isobaric cooling is documented by the replacement of sillimanite by kyanite and ilmenite by rutile (Fig. 3).

Sample **VMT-04** comes from a large block of a retrogressed granulite facies metasediment exposed on the southern flank of Monte Senevedo, not far above the saddle just to the northeast of and above Lago Pirola (GPS co-ordinate 46°18'12 N, 009°47′43 E, 2388 m). The block is part of the detritus coming from the slopes of Monte Senevedo above. The granulite facies assemblage is highly retrogressed to chlorite and micas. The original mineral assemblage was dominated by quartz, feldspar and garnet, with minor biotite. Garnet is almost completely replaced by chlorite, and feldspar is heavily altered but relict polysynthetic twins indicate that much of it is plagioclase. Quartz is partly recrystallised to mosaics of smaller crystals. Small rutile exsolution needles are visible in some quartz crystals, indicating high crystallisation temperatures. This sample was chosen because it contains abundant zircon as an accessory mineral.

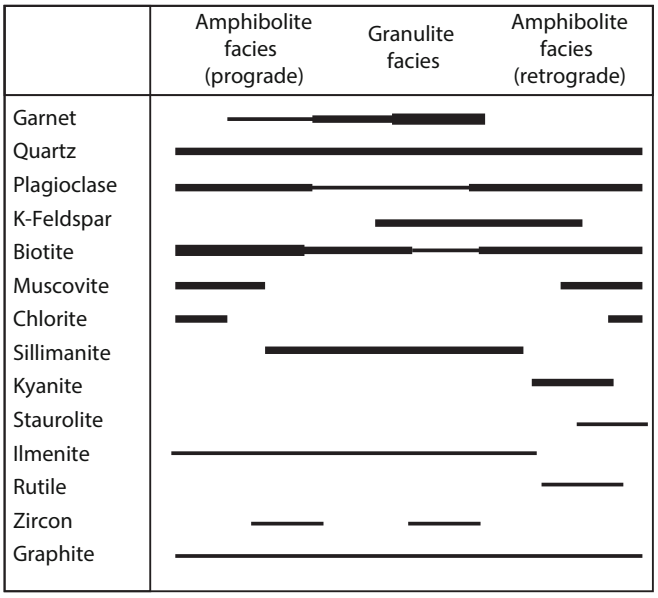

Fig. 3. Paragenesis diagram of the felsic metapelites with respect to prograde amphibolite, peak granulite and retrograde amphibolite facies metamorphism.

4. Methodology

4.1. Sample preparation and imaging

Samples were sawed into small blocks then disaggregated by high voltage using a SelFrag at the University of Bern. ~1.4 kg and ~0.7 kg of samples VMT-04 and VMT-11B respectively were disaggregated, then sieved. Zircon was separated from the 65–250 μm fraction of each sample using standard density and magnetic techniques, with a Frantz isodynamic magnetic separator and the heavy liquid methylene iodide. Zircons were hand-picked, mounted in epoxy along with zircon standards and polished to reveal their mid-sections. Zircons were imaged in reflected and transmitted light on a standard petrographic microscope, and by charge contrast (CC) imaging on a ZEISS EVO50 scanning electron microscope (SEM) at the Institute of Geological Sciences, University of Bern, at low vacuum conditions (18 Pa), 12 kV, a beam current of 700–750 pA and a working distance of 10–11 mm. CC imaging gives images equivalent to cathodoluminescence (Fig. 4). Post-analysis imaging of spot positions was carried out on the same SEM using combined secondary and backscattered electrons (BSE) and similar working conditions (12 kV, 750 pA and a working distance of 9.5 mm). The mineralogy of selected inclusions in zircons was identified by EDS analysis (targeted in backscattered electron mode) on the same SEM, after SIMS analysis.

4.2. U-Pb geochronology of zircon

Zircon U-Pb dates were measured on a Cameca IMS 1280HR in the SwissSIMS laboratory at the University of Lausanne, Switzerland. Analytical protocol broadly followed Whitehouse and Kamber (2004).

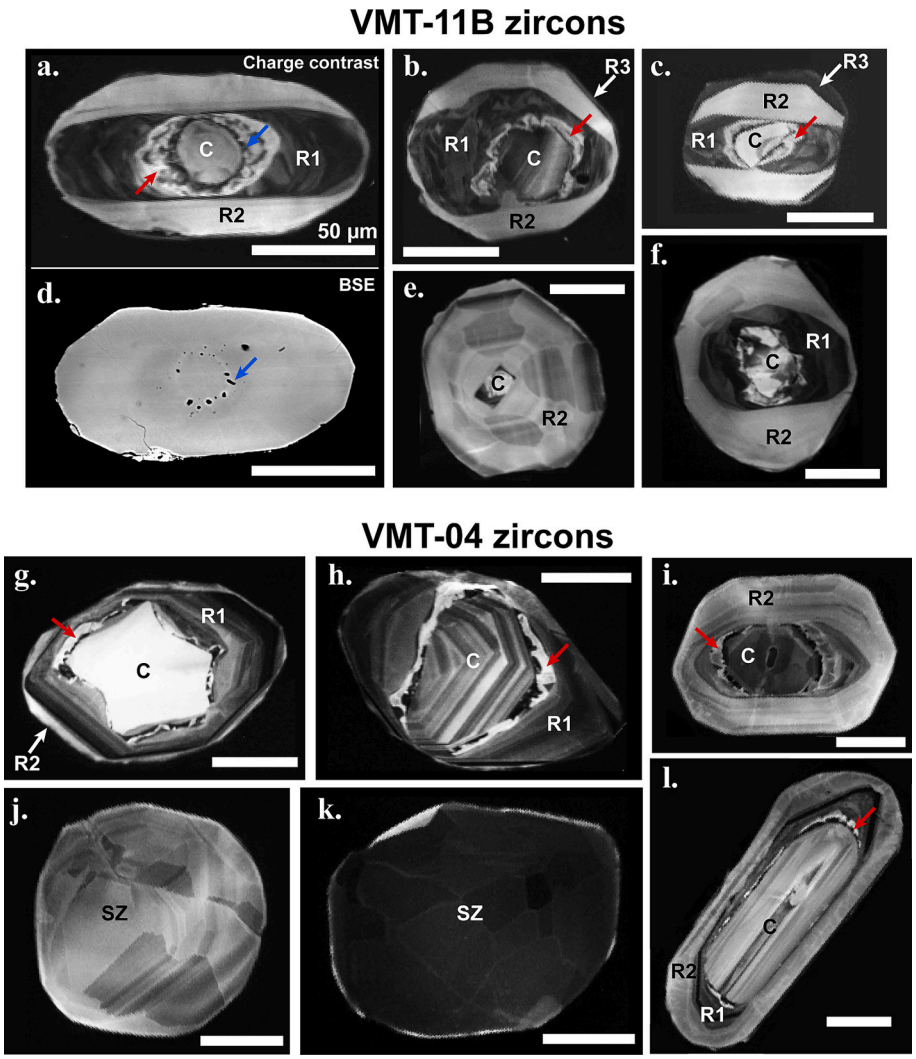

Fig. 4. Internal features of Malenco metapelite zircons, revealed by CC and backscattered electrons (d only, BSE) images. Zircons are from samples (a–f) VMT-11B and (g–l) VMT-04. Detrital cores are marked "C", and red arrows indicate the location of irregular rings of homogeneous bright or dark emission that are rich in inclusions and holes, collectively interpreted as zones of dissolution–reprecipitation that immediately surround detrital cores (see text). Different generations of metamorphic zircon growth are also distinguished: Rim 1 ("R1"), Rim 2 ("R2"), Rim 3 ("R3") and soccerball zircons ("SZ"). (d) shows a BSE image of the same zircon pictured in (a), illustrating the numerous inclusions and holes associated with the innermost part of the dissolution–reprecipitation ring (blue arrows indicate this same part of the zircon in both (a) and (d)). Scale bar is 50 µm in all images. (For interpretation of the references to colour in this figure legend, the reader is referred to the web version of this article.)

U-Pb analyses were conducted with an O_2^- primary beam with 10 kV acceleration and a ~20 µm spot size. Analysis was performed at a mass resolution M/ΔM of ~5000, an energy window of 50 eV, and primary beam currents of 3–7 nA. Temora zircon was used as a primary age standard (417 Ma, Black et al., 2003) and 91500 zircon (1065 Ma, Wiedenbeck et al., 1995) was analysed as a secondary standard. U-Pb data were processed with the CIPS program written by Martin Whitehouse using a $^{206}Pb/^{238}U$ versus UO_2/U calibration on data ^{204}Pb-corrected for common Pb. Calibration slopes for the five sessions ranged from 1.0 to 1.3, with 1σ uncertainties of 0.7–1.9% (Table S4). The calibration uncertainty was propagated onto individual analyses by the CIPS program. All data were ^{204}Pb-corrected for common Pb assuming a modern-day model Pb isotope composition (Stacey and Kramers, 1975). 91500 zircon gave concordia ages ranging from 1052 ± 9 Ma to 1068 ± 6 Ma (2σ; Fig. S1, Table S6).

After the first SIMS session, the epoxy mount was sanded down to expose a deeper level within the zircons and remove the previous SIMS pits, then repolished and re-imaged in CC, reflected and transmitted light. This approach allowed core domains that were too small to fit multiple SIMS spots laterally to be re-analysed in subsequent sessions. SEM or reflected light microscope images were carefully overlaid on each CC image, to precisely determine the location of each SIMS spot relative to the internal zoning of the zircons, and thus identify any analyses compromised by inadvertent mixing of core and rim domains, or accidental analysis of inclusions.

Dates are referred to in the text at the 2σ level, and ages at 95% confidence. Concordia diagrams, probability density plots (PDPs) and weighted averages were calculated and plotted using Isoplot 3.7 (Ludwig, 2012; Sircombe, 1999). Histograms on PDPs were constructed with a bin size close to the average 2σ uncertainty on SIMS analyses. Kernel density estimate (KDE) plots were made for comparison using DensityPlotter (Vermeesch, 2012). PDPs and KDEs were plotted using a combination of $^{207}Pb/^{206}Pb$ and $^{206}Pb/^{238}U$ dates with a threshold of 1000 Ma (assessed on $^{206}Pb/^{238}U$). The $^{207}Pb/^{206}Pb$ date was always used for >10% discordant zircons, which were interpreted to have been affected by Pb loss (see below). Concordance was assessed between the $^{207}Pb/^{235}U$ and $^{206}Pb/^{238}U$ systems for analyses with a $^{207}Pb/^{235}U$ date <1000 Ma, and between the $^{207}Pb/^{206}Pb$ and $^{206}Pb/^{238}U$ systems for ≥1000 Ma dates (see Online Appendix S1).

4.2.1. *Filtering of zircon detrital core data for discordance and isotopic disturbance*

A variety of approaches have been used to filter detrital datasets for discordant analyses. An arbitrary threshold of concordance, in many cases 5% or 10%, is commonly used (e.g. Andersen et al., 2011; Manzotti et al., 2015; Shaanan et al., 2019; Sircombe, 2004; Talavera et al., 2012), but can have a significant influence on the data interpretation (e.g. Malusà et al., 2013; Nemchin and Cawood, 2005 ; Spencer et al., 2016). Alternatively, a stricter filter for discordance can be applied by either filtering by probability of concordance (Ludwig, 1998), or accepting data that are concordant within analytical uncertainty at a confidence level such as 2σ (Spencer et al., 2016). A problem of this approach is that

it preferentially excludes more precise analyses in favour of low precision analyses that are within error of concordance (Nemchin and Cawood, 2005). Which is the most appropriate approach to deal with discordant analyses depends in part on the purpose of the study: a stricter filter is required for applications in which the relative proportions of different age peaks are important, or which aim to precisely constrain the age of specific age components in the detrital spectra, while a more lenient discordance filter is advised for applications in which detecting all (or specific) age peaks is more important than their relative proportions (Gehrels, 2014; Spencer et al., 2016).

A potential problem in using detrital zircon cores in high-grade metasediments is the possibility that they have suffered Pb loss during high-grade metamorphism subsequent to their deposition, which could result in detrital cores giving apparent (disturbed) ages younger than the real depositional age. Nemchin and Cawood (2005) observed many cases of variable degrees of discordance for different analyses of the same zircon grain in a Neoproterozoic psammite. In order to accurately constrain a maximum depositional age, multiple U-Pb analyses on individual zircons are required, if necessary by repolishing to allow reanalysis, to identify zircons affected by Pb loss (Nemchin and Cawood, 2005; Spencer et al., 2016). In this study we adopted the recommended (e.g. Coutts et al., 2019; Daniels et al., 2017; Nemchin and Cawood, 2005; Spencer et al., 2016) two-part approach: (i) a large number of analyses are used to characterise the detrital age spectrum (≥10% discordance filter), (ii) the youngest zircons are subjected to multiple analyses (accepting only concordant $^{206}Pb/^{238}U$ and $^{207}Pb/^{235}U$ dates within 2σ uncertainty).

4.3. Trace element analysis of zircon

Trace element concentrations of zircon were measured by laser ablation inductively coupled plasma mass spectrometer (LA-ICPMS) using a Resonetics RESOlutionSE 193 nm Excimer laser (Applied Spectra, USA) coupled to an S-155 large-volume constant-geometry chamber (Laurin Technic, Australia) and an Agilent 7900 ICP-QMS at the University of Bern. Standard analytical and data reduction protocols were employed, as detailed in Online Appendix S3. The spectra of trace element analyses were carefully controlled for any evidence of mixing of different domain types or contamination by inclusions, as identified by zoning of trace elements or raised concentrations of elements such as P, Sr or ^{208}Pb. The very small detrital cores in VMT-11B zircons were particularly challenging to analyse and 19 out of 47 analyses had to be discarded.

Measured concentrations of secondary standards were compared to the reference values of Jochum et al. (2005) for GSD-1G (Table S2). For 91500 the reference values were taken from Wiedenbeck et al. (1995) for Hf, Szymanowski et al. (2018) for Ti, and Wiedenbeck et al. (2004) for other elements (Table S3). The results for 91500 zircon and GSD-1G glass confirm the accuracy of our zircon trace element measurements and demonstrate that our Ti concentrations in zircon have accuracy of 10% or better. Measured concentrations in 91500 zircon were within better than 20% of reference values for all analyses of most elements (Table S2). Ti concentrations measured on 91500 zircon were always within 11% of the reference value of Szymanowski et al. (2018). The average of all measured 91500 Ti concentrations is within 0.1% of the reference value (Table S2). Concentrations measured on GSD-1G were within 20% or better of reference values for all analyses of all elements (Table S3). Ti concentrations measured on GSD-1G were systematically lower than, but always within 6–11% of, the reference value of Szymanowski et al. (2018).

4.4. Ti-in-zircon thermometry

Our analysed samples have appropriate mineral assemblages for application of Ti-in-zircon thermometry to zircon overgrowth domains: both samples are quartz-bearing and also contain both ilmenite and rutile (± titanite) as titanium phases (Section 3). Ilmenite was the stable Ti-phase at granulite facies conditions (Fig. 3). We therefore calculated Ti-in-zircon temperatures for an a_{TiO2} of 0.5 according to the calibration of Ferry and Watson (2007). The Ferry and Watson (2007) formulation is effectively calibrated for 1 GPa, which is comparable to the peak metamorphic pressures of the Malenco granulites (Hermann et al., 1997; Müntener et al., 2000).

Approximate precision of Ti-in-zircon temperatures for metamorphic domains was estimated by combining in quadrature an analytical uncertainty (taking a conservative estimate of 15% for accuracy of Ti measurements by LA-ICPMS) and the uncertainty inherent in the calibration of Ferry and Watson (2007), giving combined uncertainties of ±18–22 °C over the temperature range of interest. The uncertainty contributions from the estimation of a_{TiO2} and pressure (P) were not included, as the calibration used explicitly accounts for both of these parameters and it is difficult to place a precision on the a_{TiO2} and P estimates used. Additionally, when comparing metamorphic domains between and within the two samples analysed, both a_{TiO2} and P can be regarded as systematic uncertainties that can be ignored for assessment of relative differences in Ti-in-zircon temperatures. An inaccuracy in a_{TiO2} of ±0.1 would make 17–26 °C difference over the temperature range of interest, and an a_{TiO2} of 1.0 instead of 0.5 would result in temperatures 60–70 °C lower.

5. Results

5.1. Zircon internal zoning

Zircons from VMT-04 and VMT-11B display central core domains that show clear textural evidence for resorption (irregular boundaries), as well as different types of overgrowth domains (Fig. 4). Core domains from both samples typically show oscillatory zoning, although a few cores from each sample show homogeneous bright emission (Fig. 4). Cores are commonly separated from overgrowths by a prominent but narrow ring of dark-emission then bright-emission zircon that is irregular and jagged in shape, and is associated with many inclusions and holes (Fig. 4a,d). These irregular, inclusion-rich rings are interpreted to record a period of dissolution–precipitation (see Section 6.1) and the term "dissolution–reprecipitation ring" is used hereafter to refer to them. Core domains are interpreted as detrital cores from the metasedimentary protolith. In VMT-04, many zircon grains preserve larger (up to 150 μm) detrital cores, while in VMT-11B most detrital cores are much smaller (typically <50 μm) and in many cases show irregular shapes suggestive of heavy resorption of pre-existing zircon in this sample (Fig. 4).

Zircons from **VMT-11B** display three types of overgrowths. A first overgrowth (Rim 1) is observed directly surrounding detrital cores and the dissolution–reprecipitation rings, and generally has an elongate form. These overgrowths always have extremely dark CC-emission and are generally unzoned (Fig. 4a,b,c,f). Rim 1 domains are surrounded by thick Rim 2 overgrowths, which always have homogeneous bright emission, with either no zoning or occasionally fir-tree sector zoning (Fig. 4a,b,c,e,f). Rim 2 domains have rounded, generally equant shape, and are the outermost domain visible on many grains. In some zircons a narrow (<5 μm) dark rim (Rim 3) overgrows Rim 2 (Fig. 4b,c). Rim 3 domains were, however, too small to be analysed for U-Pb age or trace element concentrations. Some VMT-11B zircons have broadly elongate form following that of detrital cores, while many zircons have equant 'soccerball' shapes and are strongly volumetrically dominated by sector-zoned Rim 2, but generally preserve at least a small fragment of detrital core (Fig. 4e,f).

Zircons from **VMT-04** also preserve Rim 1, Rim 2 and Rim 3 generations of overgrowths, although with some important differences from VMT-11B. Rim 1 in VMT-04 is less well-developed than in VMT-11B, in many cases forming much smaller domains, and is completely absent from many grains in which Rim 2 directly surrounds detrital cores and

the dissolution–reprecipitation rings (Fig. 4g,h,i,l). Rim 2 is the best developed overgrowth in VMT-04, and is generally unzoned or sector-zoned, more rarely oscillatory zoned (Fig. 4i,l), with widely varying emission from bright to dark. A narrow (<5 μm) Rim 3 with homogeneous bright emission surrounds Rim 2 on some grains. VMT-04 also contains a number of zircon grains with equant shapes, and no detrital core (Fig. 4j,k). These soccerball zircons are made up almost entirely of a single domain with characteristics similar to Rim 2 (Fig. 4j,k) and in many cases are surrounded by a bright, narrow (<5 μm), irregular rim comparable to Rim 3. The more variable characteristics of different overgrowth generations in VMT-04 zircons make the assignment of individual domains to a particular generation based on CC images less clear than for VMT-11B zircons.

In both samples VMT-04 and VMT-11B, inclusions in dissolution–reprecipitation rings are dominated by quartz and biotite, with muscovite present only in zircon from sample VMT-11B. EDS spectra revealed that some of the biotite inclusions from both samples had high Ti contents, although other biotite inclusions had no detectable Ti. A few plagioclase inclusions were found in dissolution–reprecipitation rings of VMT-11B zircons, but were not observed in VMT-04.

5.2. Trace element geochemistry of zircon

In both VMT-11B and VMT-04 zircons, Core, Rim 1 and Rim 2 domains have clearly distinct trace element geochemistry (Fig. 5, Fig. 6, Fig. 7, Table S1). The geochemistry of each domain type is similar across the two samples, which are therefore discussed together below.

Core domains have steep heavy rare earth element (HREE) patterns (Fig. 5a), with Lu_N/Sm_N (the subscript N indicates normalisation to the chondrite values of McDonough and Sun, 1995) of 24–293 (Fig. 5a,c; Fig. 6). Only two core domains from VMT-04, both with homogeneous bright CC emission typical of metamorphic zircon, have much flatter HREE patterns with Lu_N/Sm_N of 8–33 (Fig. 5c). Cores have variable Eu anomalies ranging from weak to pronounced (Fig. 5a,c), with Eu/Eu* of 0.03–0.77 (Table S1). They have high Th/U of 0.2–2.1, with one outlier from VMT-04 at 0.07 (Fig. 6), and Ti concentrations of 5.6–13.4 ppm (Table S1).

Rim 1 domains have even steeper HREE patterns than cores, with Lu_N/Sm_N of 590–1310 (Fig. 5b,d, Fig. 6, Fig. 7). They have relatively weak Eu anomalies (Fig. 5b,d) with Eu/Eu* of 0.16–0.24 (Fig. 7a,b), and extremely low Th/U of 0.003–0.010 (Fig. 6, Fig. 7e,f). Rim 1 domains in VMT-11B have Ti concentrations of 4.8–7.1 ppm, corresponding to Ti-in-zircon temperatures of 740–780 °C (calculated as described in Section 4.4 using the calibration of Ferry and Watson, 2007) (Fig. 7c,e). Rim 1 domains in VMT-04 have Ti concentrations that are higher on average, with 7.0–9.2 ppm, giving Ti-in-zircon temperatures of 780–810 °C (Fig. 7d,f).

Rim 2 domains have relatively flat, negatively sloping or slightly concave HREE patterns with Lu_N/Sm_N of 0.8–11 (Fig. 5b,d, Fig. 6, Fig. 7). Two Rim 2 analyses from VMT-04 have a steeper HREE pattern with Lu_N/Sm_N of 54 and 166 (Fig. 5d, Fig. 6, Fig. 7). Rim 2 domains in VMT-04 show greater variability in absolute HREE concentrations than Rim 2 in VMT-11B (Fig. 3d, cf. Fig. 3b). Rim 2 domains from both samples have pronounced Eu anomalies (Fig. 5b,d) with Eu/Eu* of 0.03–0.08 (Fig. 7a,b). They have low Th/U that is intermediate between that of Core and Rim 1 domains, ranging from 0.009 to 0.14 (Fig. 6,

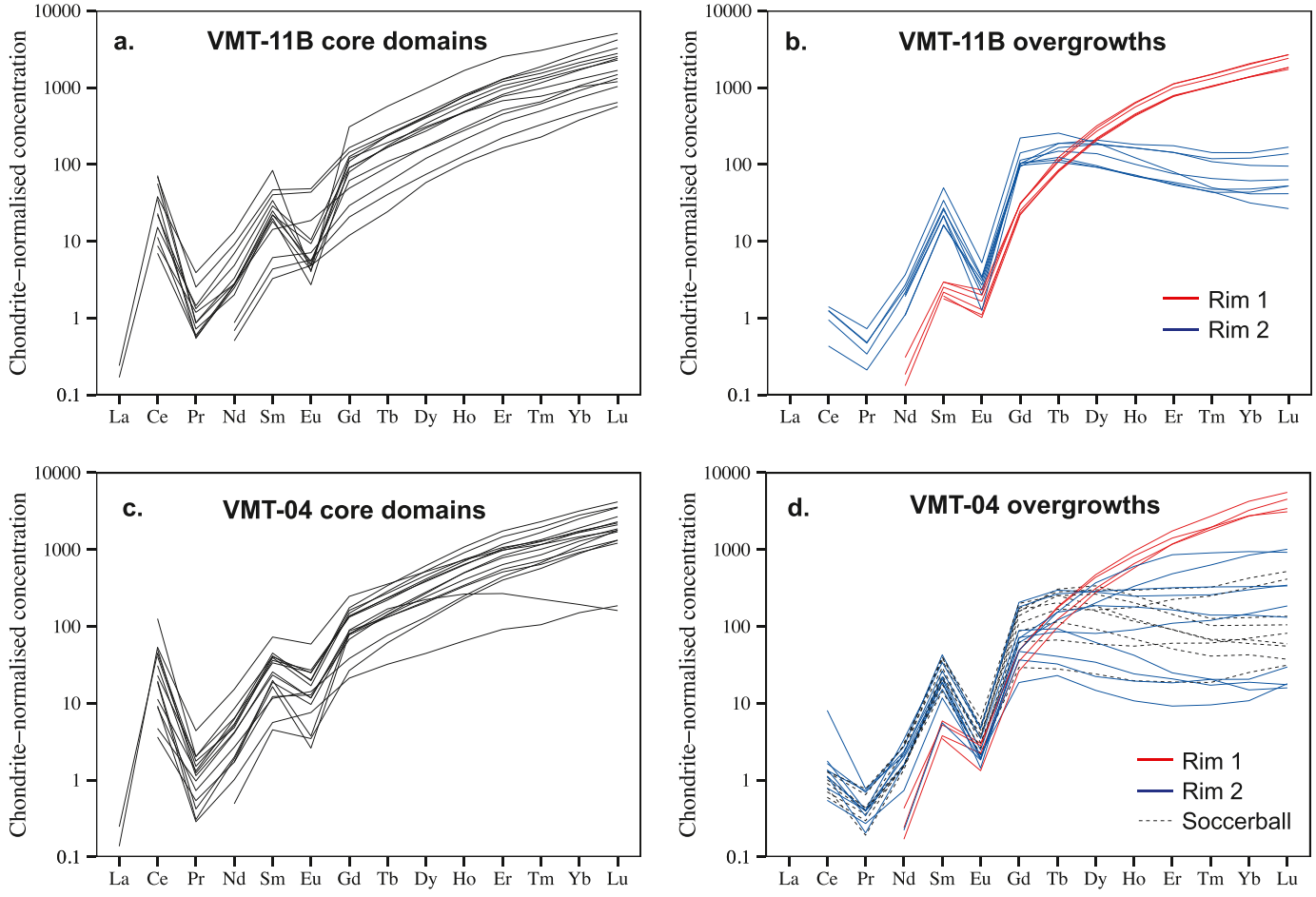

Fig. 5. Rare earth element concentrations for zircons from Malenco granulites, normalised to the chondrite values of McDonough and Sun (1995). Line colours and stroke distinguish different internal domains within zircons.

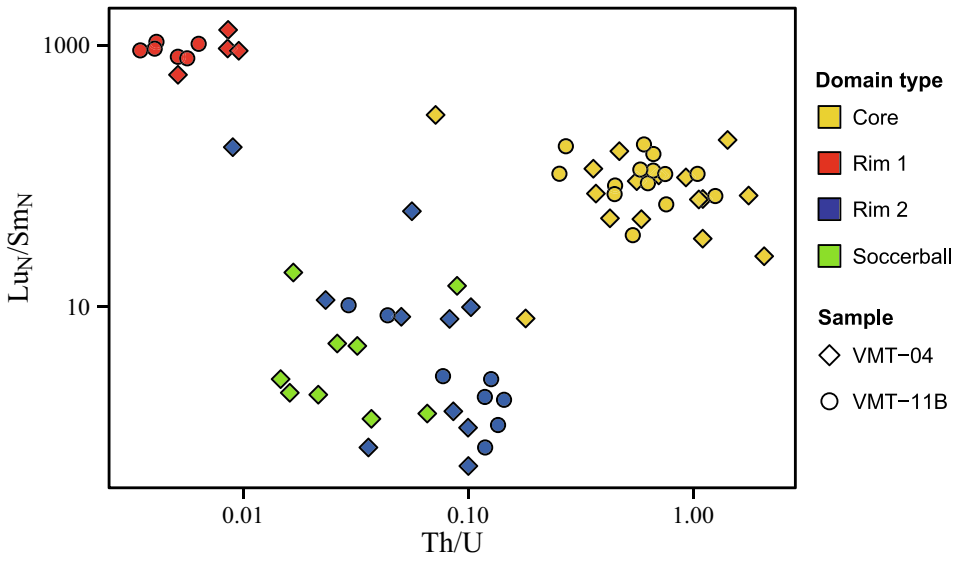

Fig. 6. Plot of Lu_N/Sm_N (ratio of chondrite-normalised concentrations) versus Th/U for samples VMT-11B and VMT-04, showing the excellent discrimination between different zircon internal domain types based on geochemistry.

Fig. 7e,f). Rim 2 Ti concentrations range from 7.4 to 9.7 ppm for VMT-11B, and 5.7–11.6 ppm for VMT-04, corresponding to Ti-in-zircon temperatures of 780–810 °C and 760–830 °C, respectively (Fig. 7c,e,d,f).

The few soccerball zircon grains, which lack core domains and are found only in VMT-04, have REE and Th/U compositions that fall within the range of Rim 2 domains: Lu_N/Sm_N of 1–18, Eu/Eu* of 0.06–0.11, and intermediate Th/U of 0.015–0.089 (Fig. 5d, Fig. 6, Fig. 7). Soccerball zircons have Ti contents of 4.7–11.6 ppm, returning Ti-in-zircon temperatures of 740–830 °C (Fig. 7d,f).

5.3. U-Pb geochronology

5.3.1. Detrital cores

5.3.1.1. Filtering of U-Pb data for zircon cores. After exclusion of ten mixed core–rim analyses identified in post-analysis imaging, data were filtered for discordance using a threshold of 10% (see Section 4.2.1). Eight core analyses from VMT-04 and four from VMT-11B were reversely discordant at the 10% level, indicating an analytical artefact or targeting problem (e.g. inclusions). These analyses were excluded and are not discussed below or shown in data tables. Ten analyses from VMT-04 cores and fourteen from VMT-11B cores were ≥ 10% normally discordant (Fig. 8). These are interpreted as cores in which the U-Pb system was disturbed by partial Pb loss. The $^{207}Pb/^{206}Pb$ dates from these analyses are between ~900–2900 Ma and give a minimum age for the detrital cores.

Probability density plots (PDPs) and kernel density estimates (KDEs) of zircon U-Pb data were constructed both including and excluding discordant analyses (Fig. 9, Fig. S3, Fig. S4, Fig. S5) to compare the two types of spectra and evaluate whether any important provenance components were missed as a result of the discordance filtering (e.g. Fedo et al., 2003; Malusà et al., 2013; Nemchin and Cawood, 2005; Reimink et al., 2016; Spencer et al., 2016). KDEs were found to work poorly for our dataset (see Online Appendix S2, Fig. S2) and are only shown for comparison in Figs. S3 and S4. We present our data as PDPs (Fig. 9, Fig. S5), which have the advantage of taking into account the analytical uncertainty of individual dates. The wide range of U contents and ages of the detrital zircon cores results in significant variation in the analytical precision of individual dates (±6–62 Ma 2σ; Table S5), and we consider this important information to be taken into account in order to accurately illustrate the *measured* age spectra. We note that our interest is not in quantifying probability density or relative proportions of different age peaks, but simply to sketch out the general form of the age spectrum and identify the major age peaks.

5.3.1.2. Detrital age spectra. Seventy-two analyses from sample VMT-04 and fifty-five analyses from sample VMT-11B are concordant at the 10% level (Fig. 8). Concordant core analyses give dates ranging from 387 ± 21 Ma (2σ) to 2055 ± 38 Ma for VMT-04, and 325 ± 8 Ma to 2380 ± 16 Ma for VMT-11B (Fig. 9a-d, Table S5). Detrital cores from VMT-04 and VMT-11B have similar age distributions on PDPs (Fig. 9), consistent with the fact that they are derived from the same metasedimentary unit. Therefore, the following discussion of age spectra considers the two samples combined (Fig. 9e,f). The combined age spectrum is dominated by 400–800 Ma dates, with a minority of dates in the range 800–1000 Ma, and a few scattered 1800–2400 Ma dates (Fig. 9e,f). The main 400–800 Ma age population is dominated on the PDP by a series of peaks at ~800 Ma, ~700 Ma, 600–550 Ma, and 500–425 Ma (Fig. 9f). The broad 500–425 Ma and 600–500 Ma peaks are defined by the most dates but do not dramatically dominate over the other peaks. Subordinate peaks at ~425–400 Ma (defined by ~10 analyses) and two distinctly younger dates at ~330 Ma represent the youngest dates in the PDP spectrum (Fig. 9f).

Discordant analyses from the two samples give $^{207}Pb/^{206}Pb$ dates of 919 ± 184 Ma to 2914 ± 40 Ma (Table S5). Inclusion of $^{207}Pb/^{206}Pb$ dates for discordant analyses as a minimum age for Pb-loss-affected cores increases the proportion of Paleoproterozoic–Archean ages by adding a significant number of dates, mainly scattered between 1500 and 3000 Ma, but does not fundamentally change the age distribution (Fig. S5).

5.3.1.3. Replicate analyses of youngest core domains for maximum depositional age. For the seven core domains in each sample that gave the youngest <10% discordant dates in the first SIMS session, replicate analyses were carried out in two subsequent sessions, after polishing the epoxy down to below the level of the original SIMS spots. This approach is recommended when precise information such as maximum depositional age is sought (Nemchin and Cawood, 2005; Spencer et al., 2016). A total of two to three replicate analyses were carried out for each young core, according to how much space was available. This rigorous approach is particularly imperative in our samples, which have experienced granulite facies metamorphism, increasing the likelihood that they have been affected by disturbance. Discordance in these youngest analyses was assessed more stringently, comparing three different dates

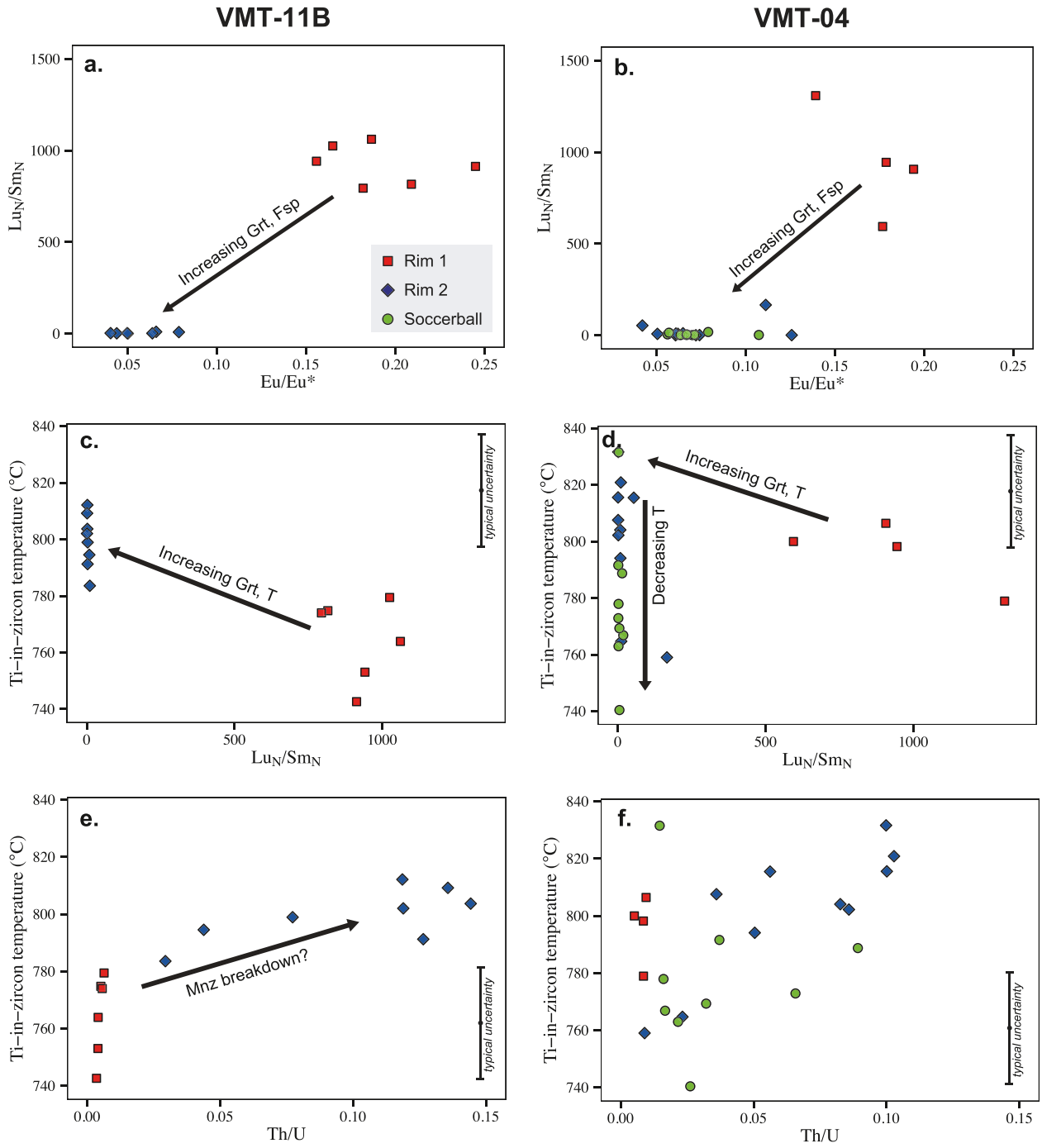

Fig. 7. Geochemical plots for metamorphic domains of zircons from samples (a,c,e) VMT-11B and (b,d,f) VMT-04. Different generations of metamorphic zircon (as discussed in text) are distinguished by symbol colour and shape. Ti-in-zircon temperatures were calculated according to the calibration of Ferry and Watson (2007) for an a_{TiO2} of 0.5. Approximate uncertainty on Ti-in-zircon temperatures (calculated as discussed in text) is indicated by an error bar at the right of plots c–f. Black arrows indicate geochemical evolution of metamorphic zircon from texturally older to younger domains, with text indicating the mineralogical controls interpreted to give rise to this evolution, as discussed in text.

($^{206}Pb/^{238}U$, $^{207}Pb/^{235}U$ and $^{207}Pb/^{206}Pb$) to check for signs of disturbance, and assessing discordance at the 2σ uncertainty level rather than the 10% level. With the exception of analyses that were excluded, as discussed below, all replicate analyses were concordant at the 2σ level in the $^{206}Pb/^{238}U$–$^{207}Pb/^{235}U$ system, although three analyses were slightly discordant (2–5%) in the $^{206}Pb/^{238}U$–$^{207}Pb/^{206}Pb$ system.

In spite of most analyses being concordant at the 2σ uncertainty level, in many cases dates for replicate analyses of the same core were ≥ 100 Ma apart (Fig. 10, Fig. S6, Fig. S7). In light of these differences, these cores were minutely re-examined for any potential inclusions or mixing of domains that could explain the different dates obtained. Where possible, EDS analysis was carried out on any inclusions with the potential to have affected the analysis.

5.3.1.4. VMT-04. The best-constrained young core age comes from VMT-04 zircon #D (Fig. 10). Two out of three analyses of this oscillatory-zoned core are concordant at the 2σ level and agree within error (Fig. 10, Fig. S6), giving a weighted mean ^{207}Pb-corrected age of 424 ± 6 Ma (MSWD = 0.1). The third analysis of this core has a $^{206}Pb/^{238}U$ date that is within error of the others (inclusion of this core

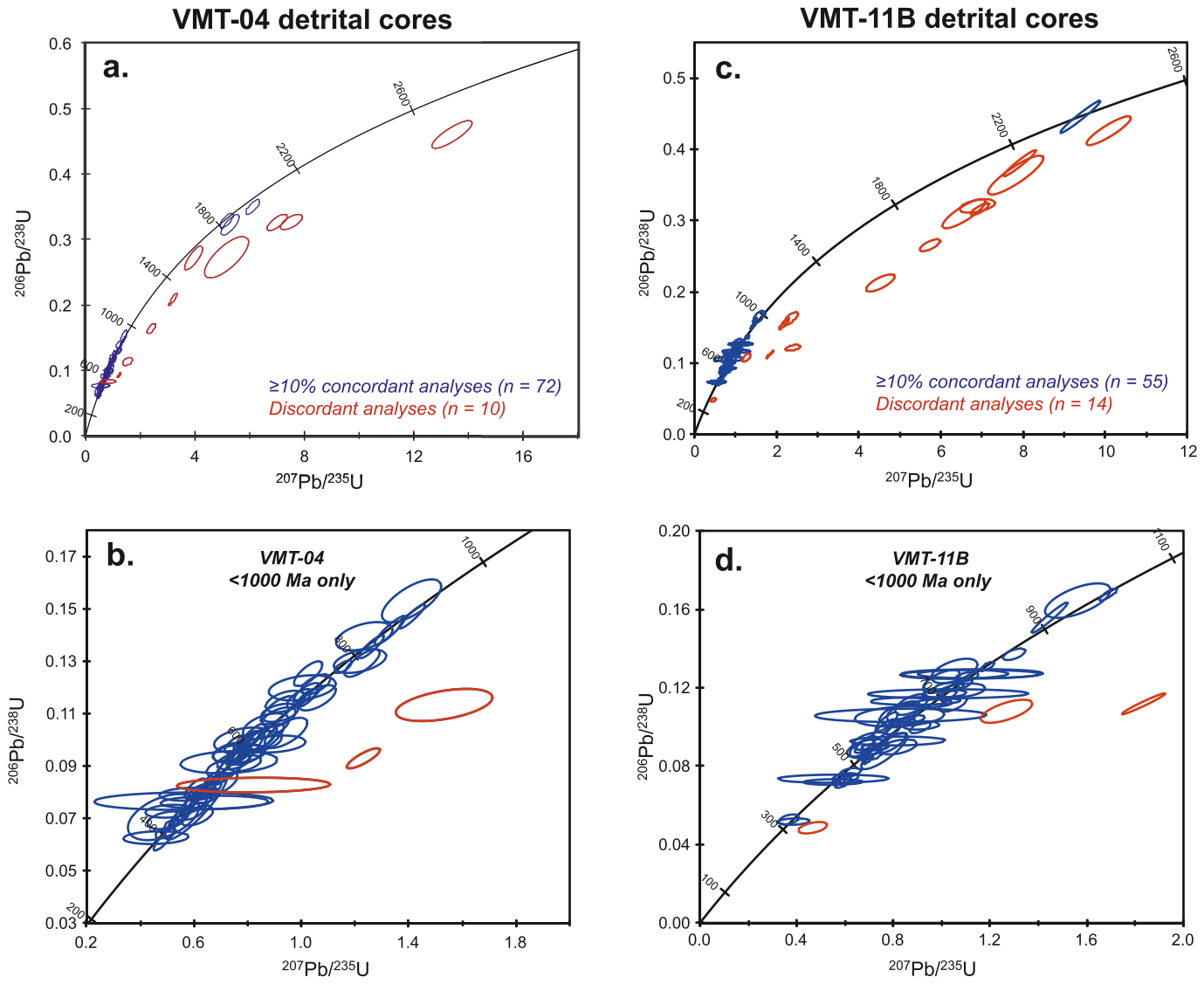

Fig. 8. Wetherill concordia plots for detrital zircon cores from (a,b) VMT-04 and (c,d) VMT-11B. Data are plotted at the 2σ level. Ellipse colour distinguishes data that are concordant (blue) or discordant (red) at the 10% level. (a,c) plot all data for each sample, while (b, d) zoom in on only <1000 Ma dates. (For interpretation of the references to colour in this figure legend, the reader is referred to the web version of this article.)

gives a weighted average of 425 ± 5 Ma, MSWD = 1.2), but its U-Pb systematics are clearly disturbed, with distinctly older $^{207}Pb/^{235}U$ and much older $^{207}Pb/^{206}Pb$ dates. Subsequent EDS analysis revealed that this spot was contaminated by an inclusion of biotite, which may be responsible for the disturbed systematics, supported by the distinctly lower precision of this analysis compared to the other two. This justifies exclusion of this analysis and, importantly, suggests its disturbed systematics do not result from partial Pb loss but rather contamination. The other two analyses are therefore regarded as robust and undisturbed, and inferred to date the detrital core formation.

Two analyses of another detrital core, VMT-04 #B, gave $^{206}Pb/^{238}U$ dates that just overlap within error at ~400 Ma, with a third analysis that is much less precise and was excluded for reverse discordance (Fig. 11, Fig. S6). The remaining two analyses gave an imprecise weighted mean of 395 ± 160 Ma with a high MSWD of 4.4. This, and the proximity of one of these two spots to the inclusion ring surrounding the core, cast doubt on whether dates of this core are undisturbed. This core is not regarded as useful for refining the maximum depositional age, noting that it in any case both dates broadly agree with the more precise weighted mean age from zircon #D.

Of two replicate analyses of detrital core VMT-04 #G, one yielded a reversely discordant date that was discarded, leaving no replicate analysis for the other date. Four other VMT-04 cores all had two or three replicate analyses that are concordant but gave dates differing well outside of error and typically by ≥100 Ma (Fig. 10A, Fig. S6). The youngest dates on these cores range from 390 to 440 Ma, while the oldest dates range from 520 to 780 Ma (Fig. 10A, Table S5).

5.3.1.5. VMT-11B. Detrital cores in VMT-11B zircons are much smaller than in VMT-04 zircons, which made them challenging to accurately target for dating even at the high spatial resolution of the SIMS. Six of the seven VMT-11B detrital cores analysed repeatedly had one of the replicate analyses that was invalidated by mixed core–rim sampling (three cores), contamination by inclusions identified in EDS to be Bt-Ms-Chl (one core), or reverse discordance (two cores). Because of their small size, only two analyses were possible for each of these cores, meaning that exclusion of one analysis made it impossible to assess whether the remaining analysis of each core could have been affected by Pb loss. Data for these six cores are therefore not plotted in Fig. 10 and S7, and these cores are not considered further for the question of the youngest detrital core age.

The one remaining VMT-11B core had initially the youngest age of

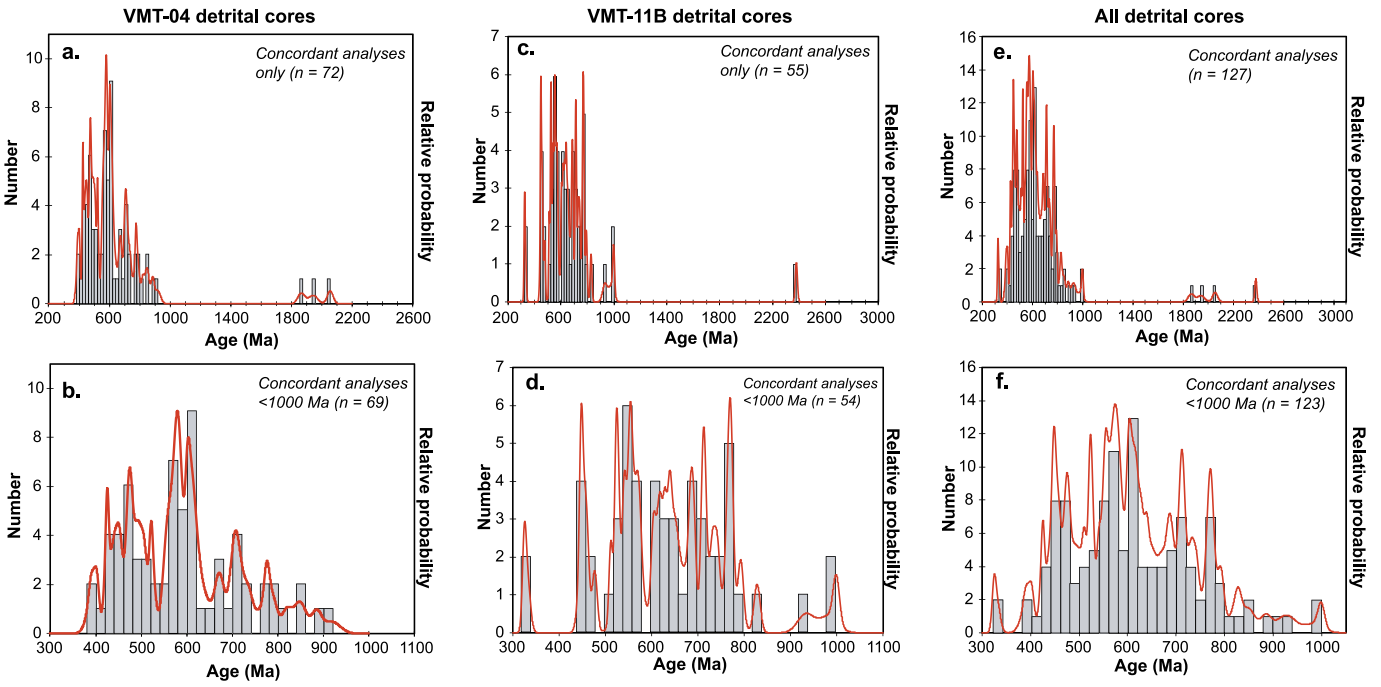

Fig. 9. Probability density plots (PDPs) for detrital zircon cores from (a,b) VMT-04, (c,d) VMT-11B and (e,f) both samples combined. PDPs were constructed using $^{207}Pb/^{206}Pb$ dates for >1000 Ma and $^{206}Pb/^{238}U$ dates for <1000 Ma (see text). Only analyses that are concordant at the 10% level are plotted. (a,c,e) all concordant analyses; (b,d,f) zoom in on <1000 Ma analyses.

~330 Ma, and two replicate analyses that gave concordant dates each differing by >100 Ma (Fig. 10b, Fig. S7). It is unclear whether the dates of this core differ so markedly due to issues with contamination by inclusions or different domains, or due to disturbance of the U-Pb system. In either case, this zircon core cannot be taken to constrain the age of the youngest detritus in this sample. Ultimately, we were unsuccessful in making a database of replicate core analyses for VMT-11B.

5.3.2. *Metamorphic rims (VMT-11B)*

Metamorphic rim domains were U-Pb dated in sample VMT-11B, to check whether our samples reproduced previous geochronological results for metamorphic zircon domains from a single sample of Malenco Unit metasedimentary granulite (Hermann and Rubatto, 2003). Sample VMT-11B was selected as it had the best-developed metamorphic domains, with both of Rim 1 and Rim 2 large enough to analyse in many zircon grains. Fifteen analyses of VMT-11B targeted both Rim 1 and Rim 2 domains, which were distinguished based on their distinct CC image characteristics (Section 5.1).

A probability density plot of all acceptable analyses of both types of metamorphic zircon domain shows a non-Gaussian distribution suggestive of a mixture of different age populations that are not well-resolved based on geochronological data alone (Fig. 11b). However, the different domain types independently identified based on CC images and trace element geochemistry each give a coherent population of U-Pb dates that relate to a single age. Five Rim 1 domains gave concordant dates that all agree within error, with a concordia age (^{204}Pb-corrected data) of 272.9 ± 2.8 Ma, and a weighted mean ^{204}Pb-corrected $^{206}Pb/^{238}U$ age of 272.9 ± 3.4 (MSWD = 1.8) (Fig. 11a,c). Eight Rim 2 domains gave a concordia age of 263.8 ± 2.6 Ma (uncertainty forced to 1% to account for long term reproducibility), which is younger than the age of Rim 1 (Fig. 11a). Rim 2 domains gave an indistinguishable weighted mean ^{204}Pb-corrected $^{206}Pb/^{238}U$ age of 263.8 ± 2.8 Ma (MSWD = 2.5) (Fig. 11a,c). Our preferred ages are the concordia ages, as they take into account isotope data from both decay schemes, and are slightly more precise (noting that they are indistinguishable from the weighted mean ^{204}Pb-corrected $^{206}Pb/^{238}U$ ages).

6. Discussion

6.1. *Nature of zircon domains*

Internal structure (observed in CC images), trace element geochemistry and U-Pb ages collectively allow several generations of zircon domains to be distinguished in VMT-11B and VMT-04. Zircons from both samples are seen to preserve partially-resorbed core domains and three generations of overgrowth domains (Rim 1, Rim 2 and Rim 3), as well as core-free soccerball zircons in VMT-04 only (Fig. 4). The outermost, texturally youngest Rim 3 domains were too small to analyse and are not discussed here.

Core domains have distinct geochemistry and U-Pb ages from all rim and soccerball domains (Fig. 5, Fig. 6). Core domains are always central domains, and in many cases have irregular boundaries that suggest partial resorption (e.g. Fig. 4). These features are indicative of a detrital origin for these domains, which is confirmed by the large spread of U-Pb dates for core domains (390–2060 Ma for VMT-04 and 330–2380 Ma for VMT-11B; Section 5.3.1, Fig. 8, Fig. 9). Detrital zircon cores in VMT-11B metapelite are seen to be particularly strongly resorbed, with much smaller sizes and more irregular boundaries compared to VMT-04 detrital cores (Fig. 4). The oscillatory zoning, high Th/U of >0.15 and steep HREE patterns of almost all core domains from both samples (Fig. 5, Fig. 6) are features typical of igneous zircon (e.g. Corfu et al., 2003; Hoskin and Schaltegger, 2003; Rubatto, 2002, 2017), indicating that detrital zircon in the protolith was overwhelmingly derived from magmatic sources. Only three of the core domains analysed for geochemistry have any features that could suggest a metamorphic origin (homogeneous bright emission in CC images for two cores, and low Th/U of 0.07 for a third core; Table S1, Fig. 6).

Overgrowth (Rim 1 and Rim 2) domains from both samples and soccerball zircons from VMT-04 are all clearly distinct from core domains in terms of both geochemistry and U-Pb age. Rim 1, Rim 2 and soccerball domains all have the low Th/U (0.003–0.14) and homogeneous or sector-zoned CC emission (Fig. 4, Fig. 6, Table S1) that typifies metamorphic zircon (e.g. Corfu et al., 2003; Rubatto, 2002, 2017). In sample VMT-11B, Rim 1 and Rim 2 metamorphic domains were dated,

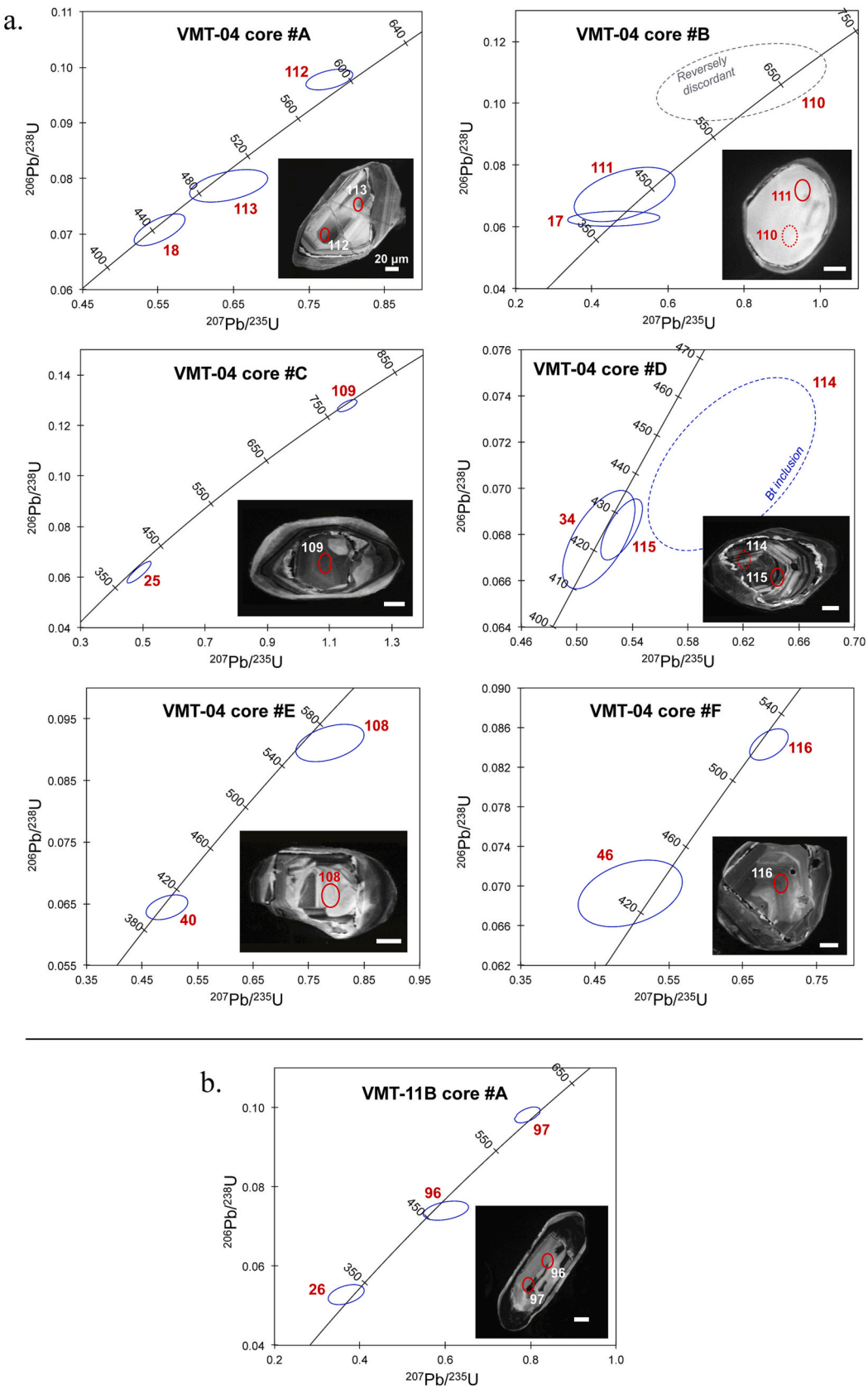

Fig. 10. Wetherill concordia plots showing replicate analyses of individual detrital cores from (a) VMT-04 (six cores) and (b) VMT-11B (one core). Each ellipse is annotated with its analysis number in red. Inset CC images show the detrital core analysed, with SIMS spot(s) marked as red ellipses annotated with analysis number. CC images were taken after repolishing to remove the pits from the first SIMS session. CC images both before and after this repolishing, and all SIMS spots, are shown for each zircon in Supplementary Fig. S6 and S7. White scale bar is 20 µm in all CC images. Data are plotted ^{204}Pb-corrected for common Pb and with 2σ uncertainties. (For interpretation of the references to colour in this figure legend, the reader is referred to the web version of this article.)

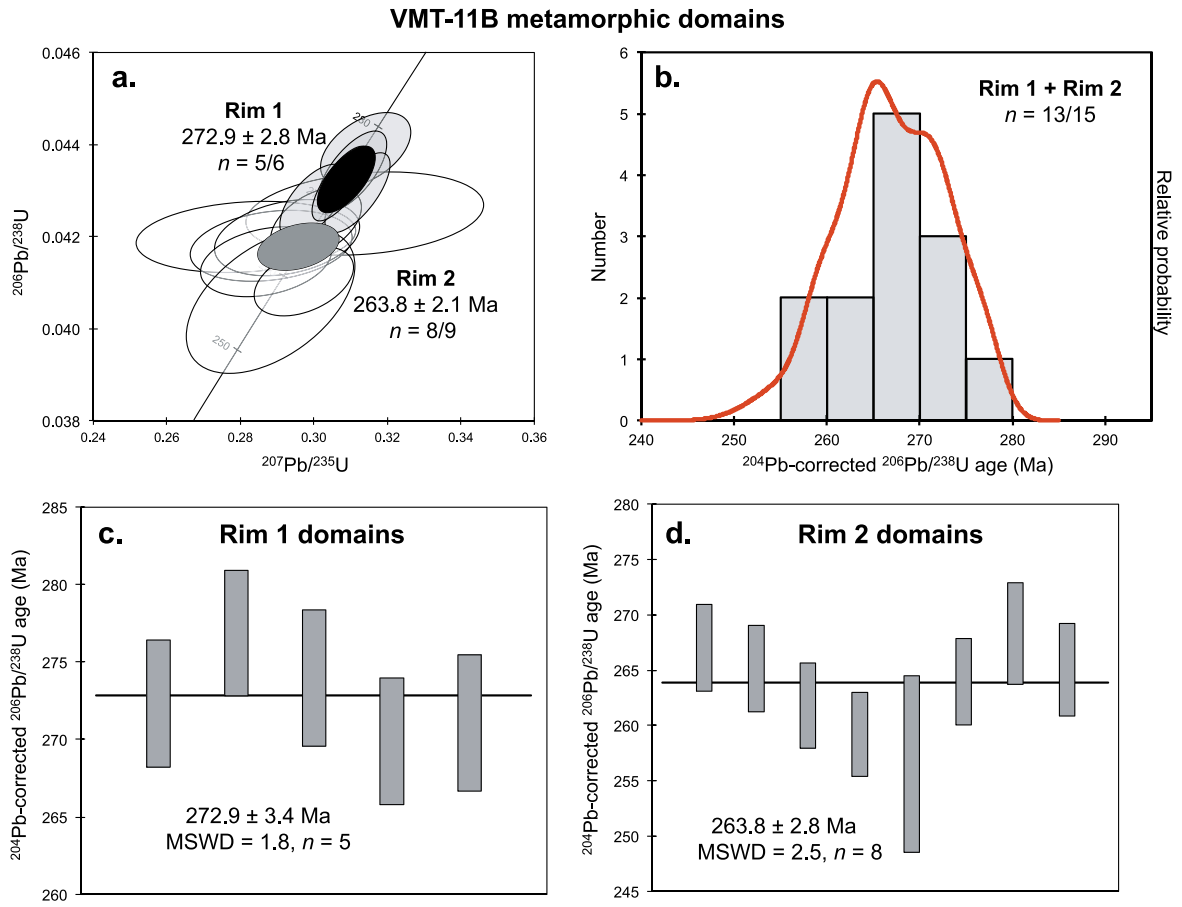

Fig. 11. U-Pb data for VMT-11B metamorphic zircon domains. Rim 1 and Rim 2 domains, identified by internal zoning as described in the text, are distinguished. (a) Wetherill concordia for ^{204}Pb-corrected data. Ellipses are plotted at 2σ, and their colour distinguishes Rim 1 (gray) and Rim 2 (white). Concordia ages are shown at the 95% confidence level and are plotted as dark opaque ellipses (black: Rim 1; dark gray: Rim 2) and given as text. (b) Probability density plot of ^{204}Pb-corrected ^{206}Pb/^{238}U dates from both Rim 1 and Rim 2 analyses. (c, d) Weighted mean ^{204}Pb-corrected ^{206}Pb/^{238}U ages (95% conf.) for (c) Rim 1 and (d) Rim 2. Gray bars represent individual dates at the 2σ level.

and collectively gave much younger U-Pb ages than any of the cores (257–277 Ma; Fig. 12, cf. Fig. 10; Table S5). Rim 1 and Rim 2 domains and soccerball zircons are therefore interpreted as metamorphic zircon formed during the Permian granulite facies metamorphism of the metapelites.

The narrow, unzoned rings of dark-emission and bright-emission zircon that separate core domains from overgrowth domains in CC images (Fig. 4a–d,g–i,l) provide a valuable independent criterium by which to identify detrital cores. The textural features of these inclusion-rich 'rings' around cores, which are irregular and jagged in shape and host many inclusions and holes (Fig. 4a–d,g–i,l), are interpreted to record a dissolution–reprecipitation event that affected detrital zircon some time after sediment burial, but prior to formation of the main metamorphic overgrowth domains. The dissolution–reprecipitation rings provide an independent marker to delineate detrital cores from metamorphic overgrowths and mean that U-Pb dates of cores can unequivocally be assigned a detrital origin. This is a valuable tool given the importance of the youngest detrital age for our study, and the fact that CC zoning alone can be ambiguous in high-grade metasediments (e.g. for central domains that have CC characteristics similar to metamorphic zircon). Similar "white seams" of <5 μm thickness have been reported from zircon in granulites from the Ivrea Zone and have been interpreted to represent the onset of zircon overgrowth on resorbed detrital grains (Vavra et al., 1996).

6.2. *Metamorphic history of the granulites recorded by zircon*

The two analysed generations of metamorphic overgrowths in both samples, Rim 1 and Rim 2, are clearly distinguished in internal zoning (Fig. 4) and also have distinctly different trace element geochemistry (e.g. Th/U, Lu_N/Sm_N, Eu/Eu*; Fig. 7a,c,e). Zircons from VMT-11B have better-developed metamorphic rims than VMT-04 zircons, and were analysed for U-Pb age as well as trace element geochemistry. Additionally, VMT-11B better preserves the granulite facies assemblage. We therefore mainly reconstructed the metamorphic history based on data from VMT-11B. Populations of dates for Rim 1 and Rim 2 domains gave distinct ^{206}Pb/^{238}U ages, with an age of 272.9 ± 2.8 Ma for Rim 1 domains and a resolvably younger age of 263.8 ± 2.6 Ma for Rim 2 domains (Fig. 11). The two generations of rims also have distinct Ti-in-zircon temperatures (Fig. 7c,e). Based on these features we interpret Rim 1 and Rim 2 to represent two generations of metamorphic zircon formed in different parts of the Permian metamorphic history.

The very steep HREE patterns (steeper than detrital cores; Lu_N/Sm_N > 500), small Eu anomalies (Eu/Eu* of 0.14–0.24) and extremely low Th/U of 0.003–0.01 of Rim 1 domains in both samples (Fig. 5b,d, Fig. 6, Fig. 7a) indicate that this generation of metamorphic zircon formed in the presence of monazite but with little garnet and no K-feldspar (e.g. Hermann and Rubatto, 2003; Rubatto, 2017). These conditions are consistent with formation during the prograde Permian metamorphic evolution, before significant quantities of garnet had been produced (Fig. 3). A prograde formation of Rim 1 is further supported by the inclusion assemblages in both zircon and garnet (studied in sample VMT-

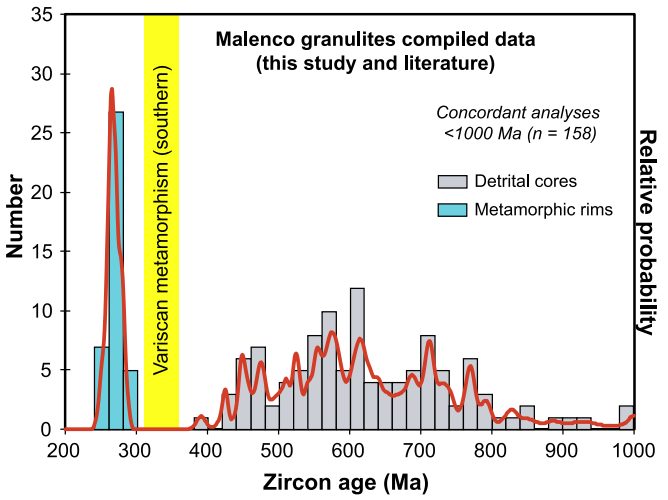

Fig. 12. Probability density plot for the compiled dataset of zircon U-Pb dates from the Malenco unit from this study (two samples) and the literature (Hermann and Rubatto, 2003; one sample). Dates for both metamorphic and detrital zircon domains are included, but only <1000 Ma dates are shown for clarity. Dates that are >10% discordant and fourteen dates from cores that were inferred to have disturbed U-Pb systematics after replicate analysis (see Section 6.3) are not plotted. The 310–360 Ma age range for Variscan metamorphism in the southern domains is based on published zircon and monazite ages from the Ivrea Zone, Southern Alps and Central Alps (Boston et al., 2017; Ewing et al., 2013; Real et al., 2023; Vavra et al., 1999), and age data for the Austroalpine reviewed by von Raumer et al. (2013).

11B). The onset of Rim 1 formation trapped quartz, biotite, plagioclase and muscovite in zircon. The mineral inclusions in garnet cores indicate that they coexisted with an assemblage of biotite, muscovite, plagioclase and quartz, typical of amphibolite facies conditions (Fig. 3). The inclusion-rich garnet cores are surrounded by voluminous and clear garnet rims containing minor sillimanite needles (Fig. 2d). This succession of distinct garnet domains documents the breakdown of muscovite and the onset of partial melting. Ti-in-zircon temperatures of VMT-11B Rim 1 domains also support a prograde formation, as they are tightly clustered at 740–780 °C (Fig. 7c,d), indicating that these domains formed at slightly higher temperatures than the onset of partial melting associated with the breakdown of muscovite, but below the peak granulite facies temperatures of 800–850 °C (Hermann et al., 1997; Hermann and Rubatto, 2003; Müntener et al., 2000). The transition from subsolidus to suprasolidus garnet in Malenco felsic granulites is further documented by trace element maps, where the M-HREE, Zr and Cr increase from core to rim, indicative of melting related to the breakdown of mica (Rubatto et al., 2020).

The highly irregular shapes and small sizes of many detrital cores in VMT-11B (e.g. Fig. 4g) testify to significant resorption, indicating that the onset of partial melting was accompanied by a period of zircon dissolution before precipitation of the first metamorphic rims began. The dissolution–reprecipitation rings observed between detrital zircon cores and Rim 1 domains also document this period of zircon resorption prior to the first metamorphic zircon growth. The 272.9 ± 2.8 Ma age for Rim 1 domains in VMT-11B thus dates the early stages of partial melting on the prograde path of the Permian granulite facies metamorphism. Texturally, Rim 1 domains are the first generation of metamorphic zircon formed around detrital cores, implying that the metapelites did not experience partial melting prior to the Permian metamorphic history, given the tendency of abundant zircon growth to begin as soon as partial melting starts (e.g. Rubatto et al., 2001). We conclude that the Malenco metapelites did not reach temperatures required for partial melting (>700 °C) until Rim 1 domains grew at 272.9 ± 2.8 Ma (Fig. 11). This age is slightly younger than the first metamorphic zircon domain of 281.4 ± 2.4 Ma but within error of the first monazite domain of 278.7 ± 4.8 Ma determined by Hermann and Rubatto (2003) in a similar sample. The U-Pb age for the Rim 1 domains is within uncertainty of the age of emplacement of the Braccia gabbro, which is most precisely constrained by the crystallisation of a partial melt segregate at 278.4 ± 2.6 Ma (Hansmann et al., 2001). The first growth of the metamorphic zircon on the prograde path therefore occurred shortly before the thermal peak associated with gabbro emplacement.

The flat REE patterns (Lu_N/Sm_N 1–18) and more pronounced Eu anomaly (Eu/Eu* of 0.03–0.13) of Rim 2 domains in both samples, as well as for the soccerball zircons in VMT-04 (Fig. 5b, Fig. 6, Fig. 7a) record growth of this generation of zircon in the presence of significant amounts of garnet and feldspar, either as peritectic K-feldspar or at the onset of leucosome crystallisation. The higher Th/U of Rim 2 domains compared to Rim 1 domains probably relates to dissolution of the Th-rich mineral monazite occurring contemporaneously with Rim 2 zircon growth (Fig. 7e). Rim 2 domains in VMT-11B have slightly hotter Ti-in-zircon temperatures of 780–810 °C than Rim 1, indicating that they formed closer to the peak temperatures of 800–850 °C attained during Permian granulite facies metamorphism associated with gabbro emplacement (Hermann et al., 1997; Hermann and Rubatto, 2003; Müntener et al., 2000). Given the discrete nature of Rim 1 and Rim 2 domains in CC images and their completely distinct trace element chemistry, protracted growth along the prograde path is not favoured and we regard growth of Rim 2 during cooling from peak temperatures as most likely. The formation of metamorphic zircon domains in two discrete events rather than by protracted growth is expected, given that Zr saturation in anatectic melts can occur at different stages of the P-T path depending on temperature, melt composition, melt extraction or injection and local equilibrium (Kelsey and Powell, 2011; Yakymchuk, 2023; Yakymchuk and Brown, 2014). In particular, two peaks in temperature have been proposed for the Malenco granulites, separated by a cooling stage (Hermann and Rubatto, 2003). Our 263.8 ± 2.6 Ma age for Rim 2 (Fig. 11) just overlaps within error with the 268.5 ± 2.6 Ma age for the second metamorphic zircon generation determined by Hermann and Rubatto (2003). The age of Rim 2 is resolvably younger than the 278.4 ± 2.6 Ma age of emplacement of the Braccia gabbro (Hansmann et al., 2001). This further supports Rim 2 zircon domains forming on the retrograde path after some cooling from the peak temperatures induced by the gabbro emplacement.

In some contexts, zircons from metapelites within the same unit have been shown to record completely different histories and geochronological data (Corvò et al., 2021), but this is not the case in the Malenco unit, where zircon records a coherent history across several metapelite samples from throughout the unit. Our two samples and the sample of Hermann and Rubatto (2003) all record similar characteristics for several generations of metamorphic zircon overgrowths, including their geochemistry and U-Pb ages. Zircon from all three samples clearly records the same response to Permian metamorphism related to the emplacement of the Braccia gabbro, irrespective of sampling location and degree of Alpine retrogression. The samples from both studies were all collected as loose blocks, so their original positions relative to the gabbro are unknown, although they sample both the northern and southern flanks of Monte Senevedo. A PDP for a compiled dataset of all reliable zircon dates from our study and the literature (Hermann and Rubatto, 2003) demonstrates the good agreement of the geochronological data from the two studies, and emphasises that the metamorphic zircon record in the Malenco relates only to the metamorphism associated with Permian gabbro emplacement, with a striking absence of Variscan ages from both metamorphic and detrital domains (Fig. 12).

6.3. *Maximum depositional age of the metasediments*

The large number of concordant analyses of detrital cores (72 for VMT-04 and 55 for VMT-11B) is close to or exceeds the 59 analyses required to be 95% confident that an age population that makes up 5%

of the age distribution has not gone undetected (Sircombe, 2004). We can therefore be confident that no major age populations were missed, and it is unlikely that the maximum depositional age would be represented by an age group that accounts for <5% of the overall age population.

Various approaches to determine the maximum depositional age from detrital zircon U-Pb data have been proposed, ranging from using the youngest single zircon date, to various calculations based on the youngest age population (e.g. the weighted mean of at least three analyses that agree at 2σ) (Dickinson and Gehrels, 2009). A host of other methods including algorithmic approaches have also been proposed but are less frequently employed (Coutts et al., 2019). Use of the youngest single grain can give a maximum depositional age that is too young, if the youngest analysis has been affected by undetected Pb loss (Dickinson and Gehrels, 2009) or if there are large numbers of near-deposition-age zircons (Coutts et al., 2019). More conservative methods involving youngest populations can give maximum depositional ages significantly older than the true depositional age compared to the youngest zircon, which can be problematic if closely approximating the true depositional age is important (e.g. in stratigraphic correlation; Coutts et al., 2019; Dickinson and Gehrels, 2009). For our samples, it is more important to safeguard against the effects of Pb loss, particularly given the high-grade metamorphic conditions experienced by the metasediments. Therefore, we consider using a single date to determine maximum depositional age to be inappropriate. Replicate U-Pb analyses were made for all of the youngest zircon cores from each sample to allow identification and exclusion of cores affected by Pb loss (Nemchin and Cawood, 2005; Spencer et al., 2016), and calculation of the maximum depositional age from a population of dates.

None of the fourteen youngest cores from the two samples (each of which were analysed 2–3 times) had all measured $^{206}Pb/^{238}U$ and $^{207}Pb/^{235}U$ dates agree within error (Fig. 10, Fig. S5). More than half of the youngest detrital cores from sample VMT-04 gave replicate analyses that were concordant at 2σ and showed no evidence for potential contamination by inclusions or mixed domains, but had $^{206}Pb/^{238}U$ dates that differed by ≥100 Ma. This implies that the majority of these youngest cores have disturbed U-Pb systematics. We therefore conclude that at least some (and probably most) of the widely differing replicate dates must result from Pb loss during high temperature metamorphism. The Pb loss could have occurred in metamorphic event(s) that affected the source lithologies prior to the detrital history of the zircons, or during the Permian granulite facies metamorphism that affected the Malenco metasediments (see above). In the latter case, the Pb loss event would post-date deposition of the sediments, and disturbed U-Pb dates for detrital cores could be younger than the depositional age of the sedimentary protolith. It is clear that these detrital cores with disturbed U-Pb systematics cannot be used to constrain the maximum depositional age of the metasediments.

For VMT-11B, no zircons gave useful replicate analyses of detrital cores, and we therefore focus on the replicate analyses of VMT-04 cores for constraining the maximum depositional age of the Malenco metasediments. The best estimate comes from detrital core VMT-04 #D, which gave the most reproducible replicate analyses of its detrital core (Section 5.3.1, Fig. 10). The weighted mean ^{207}Pb-corrected age of 424 ± 6 Ma for these core analyses is the best available constraint on the maximum depositional age of the sedimentary protolith of the Malenco granulites. The only other detrital core to give replicate analyses that agree within error, VMT-04 #B, gave two dates that broadly agree with this age, but its imprecise weighted mean age (395 ± 160 Ma) does not provide any useful further constraints on the maximum depositional age. The 424 ± 6 Ma age determined from the youngest core with reproducible dates also coincides with the first significant population on the VMT-04 probability density plot, which is a double peak at ~425 Ma and ~450 Ma (Fig. 9b). The only younger population on the PDP for VMT-04, a small peak at ~400 Ma (Fig. 9b), is defined by concordant analyses of cores that proved to have disturbed U-Pb systematics after replicate analysis (Fig. 10), and this peak largely disappears when these analyses are removed (Fig. 12).

In VMT-11B, a strong peak at ~450 Ma is the first major detrital age population (Fig. 9d). Only two analyses of this sample gave younger dates, at ~330 Ma. Replicate analyses of one of these young dates (VMT-11B #A; Fig. 10) gave dates that were ≥ 120 Ma older, indicating that the ~330 Ma core date is not a reliable age. Both of the analyses with ~330 Ma dates came from small cores where it was difficult to be certain whether the analysis was completely clear of the inclusion ring, and there are no other analyses from either sample that gave <400 Ma dates. Therefore, we do not regard ~330 Ma as a geologically meaningful age population for the detrital cores of the Malenco metapelites. Elsewhere in the Alpine realm, metasediments that sampled the widespread Carboniferous magmatic rocks in their source regions have detrital age spectra dominated by 340–330 Ma dates (e.g. Manzotti et al., 2016), so it is unlikely that metasediments that sampled these sources would record only scarce ~330 Ma dates. A PDP plotting compiled zircon U-Pb data from our study and Hermann and Rubatto (2003) with all dates from cores with disturbed systematics (as discussed above) removed shows a significant age gap of ca. 100 Ma between the youngest detrital core date and the oldest dated metamorphic overgrowth, and emphasises a complete lack of Variscan ages in both the detrital and metamorphic records (Fig. 12).

The observation that many of the youngest U-Pb dates have been affected by cryptic Pb loss cautions against using the approach of a weighted mean of the youngest major population of zircon dates (Dickinson and Gehrels, 2009) in high-grade samples. This is particularly important given that disturbed analyses were only identified when replicate analyses of the same core were carried out. We note qualitatively that in the probability density plot for both samples combined a very significant peak at ~450 Ma is the youngest major population, and clearly dominates over a smaller population at ~425 Ma (Fig. 9f, Fig. 12). Given the dominance of the ~450 Ma peak over the ~425 Ma peak in the combined PDP for both samples, a more conservative estimate of the maximum depositional age would be ~450 Ma (Ordovician). Whether the more precise age of 424 ± 6 Ma or the more conservative estimate of ~450 Ma is taken, these ages correspond to during (~450 Ma) or just after (~425 Ma) the Cenerian orogeny that affected the basement of the European Alps culminating in the Ordovician (Zurbriggen, 2017).

6.3.1. *Implications for depositional age studies in high-grade metasediments*

The observation that in our samples many of the youngest detrital zircon dates were concordant but came from cores with disturbed U-Pb systematics, as identified by replicate analyses with concordant $^{206}Pb/^{238}U$ dates >100 Ma apart, emphasises the importance of a cautious approach to determining maximum depositional age from single detrital zircon dates. This is particularly true of high-grade metasediments that are Paleozoic or younger, in which any disturbance of the U-Pb system during metamorphism is likely to result in apparently concordant U-Pb dates given the precision of 1–2% typical for in situ geochronology.

The coherent trace element geochemistry and age for each generation of metamorphic zircon in Malenco metapelites (Hermann and Rubatto, 2003; this study) contrasts with results from the Ivrea Zone (Southern Alps), where residence of metapelites at granulite facies temperatures for tens of Myr led to extensive resetting of the U-Pb system in metamorphic zircon domains, resulting in completely decoupled U-Pb age and trace element signatures, and U-Pb ages that are not coherent within each generation of metamorphic zircon overgrowths (Ewing et al., 2013; Kunz et al., 2018). The fact that even young metamorphic zircon domains in the Ivrea metasediments were affected by U-Pb resetting suggests that many of their detrital zircon cores are likely to have disturbed U-Pb ages, and single detrital zircon dates without replicate analyses (e.g. Wyatt et al., 2022) cannot be trusted to give reliable constraints on the depositional age of the Ivrea metasediments.

In our samples, replicate analyses of cores were only made possible by using SIMS measurements for U-Pb geochronology. The high spatial resolution of this technique, and in particular the very shallow pits drilled compared to LA-ICPMS, allowed repolishing of the sample to obtain replicate analyses in a subsequent session even on small cores. Without the rigorous approach of obtaining replicate analyses for all of the youngest cores (following Nemchin and Cawood, 2005; Spencer et al., 2016), the disturbed U-Pb systematics of many of the youngest cores in our samples would not have been identified, and the maximum depositional age would erroneously have been inferred to be ~400 Ma or younger. This incorrect age is tens of Myr younger than the real maximum depositional age, and belongs to a separate orogenic cycle, and would thus have strongly influenced the conclusions made from our study. We note, however, that this type of cryptic post-depositional Pb loss is a particular problem for high-grade metasedimentary samples, which are not the typical target for this type of detrital zircon study.

6.4. Implications for formation of felsic lower crust

The metamorphic history of the granulites (Section 6.2) combined with the record of inherited detrital zircon cores provide clear evidence that the Malenco granulites formed from former pelitic sediments that were subsequently buried to approximately 30 km depth. U-Pb ages of the first generation of metamorphic zircon, Rim 1 domains, are within error of the age of gabbro emplacement in the lower crust (this study; Hermann and Rubatto, 2003) but their Ti-in-zircon temperatures indicate formation on the prograde path. At the border between detrital zircon cores and metamorphic overgrowths, inclusions of muscovite, biotite and plagioclase are observed. HREE patterns of the metamorphic zircon Rim 1 are steep, indicating that only a limited amount of garnet was growing at the time Rim 1 formed. Together with the inclusion mineralogy, this provides evidence that the metapelites resided at lower amphibolite facies conditions until the gabbro intrusion generated heating and partial melting. This means that in the time period from the maximum depositional age of 425 ± 6 Ma to gabbro intrusion at ~280 Ma, the sediments must have been transported to ~30 km depth without extensive garnet formation and partial melting. Garnet cores contain plagioclase inclusions, and sillimanite needles are included in garnet rims, indicating that prior to granulite facies there was no high-pressure metamorphism, which would have stabilised kyanite instead of sillimanite and consumed plagioclase to form jadeite. Therefore the relamination model of Hacker et al. (2011) cannot explain the genesis of felsic lower crust in the Malenco case.

The felsic granulites in Malenco and the Ivrea Zone are often regarded as equivalent (Müntener et al., 2000; Staub, 1917). A recent study of the assembly of the Ivrea felsic lower crust was based on detailed investigation of monazite in amphibolite to granulite facies metapelites (Wyatt et al., 2022). They found that the oldest peak metamorphic monazite from regional metamorphism associated with burial of the metasediments is 316 ± 2 Ma, predating the intrusion of the gabbroic complex by circa 30 My. Wyatt et al. (2022) inferred a maximum depositional age of the protolith of Ivrea Zone metasediments from the 352 ± 16 Ma youngest date for detrital zircon cores in similar metapelites (Kunz et al., 2018). We note that this single LA-ICPMS detrital zircon date without replicate analyses could have disturbed U-Pb systematics (see Section 6.3.1), and the inferred maximum depositional age could therefore be too young. Based on the small time difference that Wyatt et al. (2022) inferred between maximum sedimentation age and first peak thermal metamorphism, they proposed that the sediments were quickly buried after sedimentation, similarly to what is observed in active continental margins. This burial rate would be overestimated if the inferred maximum depositional age was too young. In contrast, in the case of the Malenco granulites there is a large time span of 100 My or more between sedimentation and granulite facies metamorphism and there is no metamorphic zircon or monazite predating the gabbro intrusion and granulite facies metamorphism.

The sedimentation of the protolith for the Malenco granulites postdates 425 ± 6 Ma. According to the paleogeographic reconstructions of Stampfli and Borel (2002) and Stampfli and Kozur (2006), the Malenco rocks were situated at the north-eastern active margin of Gondwana at 420 Ma (e.g. see Fig. 1 of Stampfli and Kozur, 2006, where Malenco is part of the Austroalpine, "AA"). This setting would provide a first opportunity for subduction-related accretion of sediments at lower crustal levels shortly after their deposition. By 400 Ma the paleogeographic reconstructions show that the Paleotethys had opened up and the Malenco and Ivrea units were part of the European Hunic terrane that was drifting northwards due to the spreading of the Paleotethys (Stampfli and Borel, 2002; Stampfli and Kozur, 2006). A second opportunity to bring sediments to the lower crust occurred at 360–340 Ma, when the European Hunic terrane collided with Laurussia. However, there is no record of this Variscan orogeny in the Malenco metapelites, with a complete absence of detrital or metamorphic zircons with Variscan ages (Fig. 12).

The Malenco metasediments did not experience any partial melting and stayed below ~650 °C (amphibolite facies) until 280 Ma, since no metamorphic zircon formed until this time. Therefore, the heating to granulite facies metamorphism at 280 Ma due to the gabbro intrusion induced extensive partial melting within these fertile metasediments associated with significant melt extraction, resulting in highly refractory garnet-rich granulites (Hermann et al., 1997).

7. Conclusions

The determination of maximum depositional ages for protoliths of felsic granulites is challenging. Detrital zircon grains are partially resorbed during the onset of partial melting resulting in small cores. Additionally, the U-Th-Pb system of detrital cores can be significantly disturbed during high temperature metamorphism. In Phanerozoic zircons, even significant disturbance may not result in resolvable discordance, so that this resetting can only be detected if zircons are analysed repeatedly. Widespread cryptic disturbance of this type has been documented in the Malenco felsic granulites by replicate analyses of individual detrital zircon cores, which gave concordant $^{206}Pb/^{238}U$ dates >100 Ma apart, emphasising the importance of a cautious approach to determining maximum depositional age from single detrital zircon dates in high grade samples.

The maximum depositional age of the protolith of the Malenco felsic granulites is determined to be 424 ± 6 Ma based on overlapping replicate analyses of a single detrital core, and there is a significant detrital zircon age population at 450 Ma. Considering the paleogeography between 430 and 280 Ma, it is plausible that sediments deposited ~420 Ma at the active continental margin of northeastern Gondwana were subducted and accreted prior to the opening of the Paleotethys and the northward drifting of the European Hunic terrane, of which the Malenco rocks were a part. There is no evidence for any metamorphic zircon overgrowth or recrystallisation of Variscan age, suggesting that the metapelites remained at subsolidus conditions while they resided in the lower crust for up to 100 My. Plagioclase inclusions in garnet cores and sillimanite inclusions in garnet rims testify to the fact that the metapelites experienced no high-pressure stage and thus the felsic lower crust in Malenco did not form by relamination.

During Permian extension and the associated intrusion of a lower crustal gabbro, the Malenco metapelites underwent granulite facies metamorphism. This is documented in two distinct metamorphic zircon overgrowths with increasing Ti-in-zircon temperatures from 740–780 °C for the prograde Rim 1 (272.9 ± 2.8 Ma), to 780–810 °C for Rim 2 (263.8 ± 2.6 Ma) that formed shortly after gabbro emplacement. From Rim 1 to Rim 2, zircon trace chemistry changed from steep HREE to flat HREE patterns with a concomitant increase of a negative Eu-anomaly, indicating the formation of peritectic garnet and K-feldspar. Therefore, the granulitisation and extensive partial melting of felsic lower crust did not occur during subduction and accretion of sedimentary material, nor

during a collisional phase, but in an extensional setting.

Declaration of Competing Interest

The authors declare that they have no known competing financial interests or personal relationships that could have appeared to influence the work reported in this paper.

Acknowledgements

We thank Thomas Pettke, Francesca Piccoli and Alfons Berger (University of Bern), and Johanna Marin-Carbonne and Anne-Sophie Bouvier (University of Lausanne + SwissSIMS) for their assistance with analytical work. We thank Antonio Langone and an anonymous reviewer for their constructive reviews that improved the manuscript, and Nadia Malaspina for editorial handling.

Appendix A. Supplementary data

Supplementary data to this article can be found online at https://doi.org/10.1016/j.lithos.2023.107286.

References

Andersen, T., Saeed, A., Gabrielsen, R.H., Olaussen, S., 2011. Provenance characteristics of the Brumunddal sandstone in the Oslo Rift derived from U-Pb, Lu-Hf and trace element analyses of detrital zircons by laser ablation ICMPS. Nor. J. Geol. Nor. Geol. Foren. 91.

Black, L.P., Kamo, S.L., Allen, C.M., Aleinikoff, J.N., Davis, D.W., Korsch, R.J., Foudoulis, C., 2003. TEMORA 1: a new zircon standard for Phanerozoic U–Pb geochronology. Chem. Geol. 200, 155–170.

Boston, K.R., Rubatto, D., Hermann, J., Engi, M., Amelin, Y., 2017. Geochronology of accessory allanite and monazite in the Barrovian metamorphic sequence of the Central Alps, Switzerland. Lithos 286–287, 502–518. https://doi.org/10.1016/j.lithos.2017.06.025.

Cawood, P.A., Hawkesworth, C.J., Dhuime, B., 2013. The continental record and the generation of continental crust. GSA Bull. 125, 14–32. https://doi.org/10.1130/B30722.1.

Corfu, F., Hanchar, J.M., Hoskin, P.W.O., Kinny, P., 2003. Atlas of zircon textures. In: Hanchar, J.M., Hoskin, P.W.O. (Eds.), Zircon. Mineralogical Society of America, Washington, DC, pp. 469–500.

Corvò, S., Maino, M., Langone, A., Schenker, F.L., Piazolo, S., Casini, L., Seno, S., 2021. Local variations of metamorphic record from compositionally heterogeneous rocks (Cima di Gagnone, Central Alps): Inferences on exhumation processes of (U)HP–HT rocks. Lithos 390–391, 106126. https://doi.org/10.1016/j.lithos.2021.106126.

Coutts, D.S., Matthews, W.A., Hubbard, S.M., 2019. Assessment of widely used methods to derive depositional ages from detrital zircon populations. Geosci. Front. 10, 1421–1435. https://doi.org/10.1016/j.gsf.2018.11.002.

Daniels, B.G., Auchter, N.C., Hubbard, S.M., Romans, B.W., Matthews, W.A., Stright, L., 2017. Timing of deep-water slope evolution constrained by large-n detrital and volcanic ash zircon geochronology, Cretaceous Magallanes Basin, Chile. GSA Bull. 130, 438–454. https://doi.org/10.1130/B31757.1.

Dickinson, W.R., Gehrels, G.E., 2009. Use of U–Pb ages of detrital zircons to infer maximum depositional ages of strata: a test against a Colorado Plateau Mesozoic database. Earth Planet. Sci. Lett. 288, 115–125. https://doi.org/10.1016/j.epsl.2009.09.013.

Ducea, M.N., Kidder, S., Chesley, J.T., Saleeby, J.B., 2009. Tectonic underplating of trench sediments beneath magmatic arcs: the Central California example. Int. Geol. Rev. 51, 1–26. https://doi.org/10.1080/00206810802602767.

Ewing, T.A., Rubatto, D., Hermann, J., 2013. The robustness of the Zr-in-rutile and Ti-in-zircon thermometers during high-temperature metamorphism (Ivrea-Verbano Zone, northern Italy). Contrib. Mineral. Petrol. 165, 757–779.

Fedo, C.M., Sircombe, K.N., Rainbird, R.H., 2003. Detrital Zircon Analysis of the Sedimentary Record. Rev. Mineral. Geochem. 53, 277–303. https://doi.org/10.2113/0530277.

Ferry, J.M., Watson, E.B., 2007. New thermodynamic models and revised calibrations for the Ti-in-zircon and Zr-in-rutile thermometers. Contrib. Mineral. Petrol. 154, 429–437.

Gehrels, G., 2014. Detrital Zircon U-Pb Geochronology Applied to Tectonics. Annu. Rev. Earth Planet. Sci. 42, 127–149. https://doi.org/10.1146/annurev-earth-050212-124012.

Hacker, B.R., Kelemen, P.B., Behn, M.D., 2011. Differentiation of the continental crust by relamination. Earth Planet. Sci. Lett. 307, 501–516. https://doi.org/10.1016/j.epsl.2011.05.024.

Hansmann, W., Muntener, O., Hermann, J., 2001. U-Pb zircon geochronology of a tholeiitic intrusion and associated migmatites at a continental crust-mantle transition, Val Malenco, Italy. Schweiz. Mineral. Petrogr. Mitt. 81, 239–255.

Hermann, J., Müntener, O., 1996. Extension-related structures in the Malenco-Margna-system: implications for paleogeography and consequences for rifting and Alpine tectonics. Schweiz. Mineral. Petrogr. Mitt. 76, 501–519.

Hermann, J., Rubatto, D., 2003. Relating zircon and monazite domains to garnet growth zones: age and duration of granulite facies metamorphism in the Val Malenco lower crust. J. Metamorph. Geol. 21, 833–852.

Hermann, J., Müntener, O., Trommsdorff, V., Hansmann, W., Piccardo, G.B., 1997. Fossil crust-to-mantle transition, Val Malenco (Italian Alps). J. Geophys. Res. Solid Earth 102, 20123–20132. https://doi.org/10.1029/97JB01510.

Hermann, J., Müntener, O., Günter, D., 2001. Differentiation of Mafic Magma in a Continental Crust-to-Mantle transition Zone. J. Petrol. 42, 189–206. https://doi.org/10.1093/petrology/42.1.189.

Hoskin, P.W.O., Schaltegger, U., 2003. The composition of zircon and igneous and metamorphic petrogenesis. In: Hanchar, J.M., Hoskin, P.W.O. (Eds.), Zircon. Mineralogical Society of America, Washington, DC, pp. 27–62.

Jochum, K.P., Willbold, M., Raczek, I., Stoll, B., Herwig, K., 2005. Chemical characterisation of the USGS Reference Glasses GSA-1G, GSC-1G, GSD-1G, GSE-1G, BCR-2G, BHVO-2G and BIR-1G using EPMA, ID-TIMS, ID-ICP-MS and LA-ICP-MS. Geostand. Geoanal. Res. 29, 285–302. https://doi.org/10.1111/j.1751-908X.2005.tb00901.x.

Kelsey, D.E., Powell, R., 2011. Progress in linking accessory mineral growth and breakdown to major mineral evolution in metamorphic rocks: a thermodynamic approach in the Na_2O-CaO-K_2O-FeO-MgO-Al_2O_3-SiO_2-H_2O-TiO_2-ZrO_2 system. J. Metamorph. Geol. 29, 151–166. https://doi.org/10.1111/j.1525-1314.2010.00910.x.

Kunz, B.E., Regis, D., Engi, M., 2018. Zircon ages in granulite facies rocks: decoupling from geochemistry above 850 °C? Contrib. Mineral. Petrol. 173, 26. https://doi.org/10.1007/s00410-018-1454-5.

Ludwig, K.R., 1998. On the treatment of concordant uranium-lead ages. Geochim. Cosmochim. Acta 62, 665–676.

Ludwig, K.R., 2012. User's Manual for Isoplot 3.75: A Geochronological Toolkit for Microsoft Excel.

Malusà, M.G., Carter, A., Limoncelli, M., Villa, I.M., Garzanti, E., 2013. Bias in detrital zircon geochronology and thermochronometry. Chem. Geol. 359, 90–107. https://doi.org/10.1016/j.chemgeo.2013.09.016.

Manzotti, P., Poujol, M., Ballèvre, M., 2015. Detrital zircon geochronology in blueschist-facies meta-conglomerates from the Western Alps: implications for the late Carboniferous to early Permian palaeogeography. Int. J. Earth Sci. 104, 703–731. https://doi.org/10.1007/s00531-014-1104-8.

Manzotti, P., Ballèvre, M., Poujol, M., 2016. Detrital zircon geochronology in the Dora-Maira and Zone Houillère: a record of sediment travel paths in the Carboniferous. Terra Nova 28, 279–288. https://doi.org/10.1111/ter.12219.

McDonough, W.F., Sun, S.S., 1995. The composition of the Earth. Chem. Geol. 120, 223–253.

Müntener, O., Hermann, J., 1996. The Val Malenco lower crust–upper mantle complex and its field relations (Italian Alps). Schweiz. Mineral. Petrogr. Mitt. 76, 475–500.

Müntener, O., Hermann, J., 2001. The role of lower crust and continental upper mantle during formation of non-volcanic passive margins: evidence from the Alps. Geol. Soc. Lond., Spec. Publ. 187, 267–288. https://doi.org/10.1144/GSL.SP.2001.187.01.13.

Müntener, O., Hermann, J., Trommsdorff, V., 2000. Cooling history and Exhumation of Lower-Crustal Granulite and Upper Mantle (Malenco, Eastern Central Alps). J. Petrol. 41, 175–200. https://doi.org/10.1093/petrology/41.2.175.

Nemchin, A.A., Cawood, P.A., 2005. Discordance of the U–Pb system in detrital zircons: implication for provenance studies of sedimentary rocks. Sediment. Geol. 182, 143–162. https://doi.org/10.1016/j.sedgeo.2005.07.011.

von Raumer, J.F., Bussy, F., Schaltegger, U., Schulz, B., Stampfli, G.M., 2013. Pre-Mesozoic Alpine basements—their place in the European Paleozoic framework. GSA Bull. 125, 89–108. https://doi.org/10.1130/B30654.1.

Real, C., Fassmer, K., Carosi, R., Froitzheim, N., Rubatto, D., Groppo, C., Münker, C., Ferrando, S., 2023. Carboniferous–Triassic tectonic and thermal evolution of the middle crust section of the Dervio–Olgiasca Zone (Southern Alps). J. Metamorph. Geol. 41, 685–718. https://doi.org/10.1111/jmg.12714.

Redler, C., Johnson, T.E., White, R.W., Kunz, B.E., 2012. Phase equilibrium constraints on a deep crustal metamorphic field gradient: metapelitic rocks from the Ivrea Zone (NW Italy). J. Metamorph. Geol. 30, 235–254.

Reimink, J.R., Davies, J.H.F.L., Waldron, J.W.F., Rojas, X., 2016. Dealing with discordance: a novel approach for analysing U–Pb detrital zircon datasets. J. Geol. Soc. 173, 577–585. https://doi.org/10.1144/jgs2015-114.

Rubatto, D., 2002. Zircon trace element geochemistry: partitioning with garnet and the link between U-Pb ages and metamorphism. Chem. Geol. 184, 123–138.

Rubatto, D., 2017. Zircon: the Metamorphic Mineral. Rev. Mineral. Geochem. 83, 261–295. https://doi.org/10.2138/rmg.2017.83.9.

Rubatto, D., Williams, I.S., Buick, I.S., 2001. Zircon and monazite response to prograde metamorphism in the Reynolds Range, central Australia. Contrib. Mineral. Petrol. 140, 458–468.

Rubatto, D., Burger, M., Lanari, P., Hattendorf, B., Schwarz, G., Neff, C., Keresztes Schmidt, P., Hermann, J., Vho, A., Günther, D., 2020. Identification of growth mechanisms in metamorphic garnet by high-resolution trace element mapping with LA-ICP-TOFMS. Contrib. Mineral. Petrol. 175, 61. https://doi.org/10.1007/s00410-020-01700-5.

Rudnick, R.L., 2018. Earth's continental crust. In: White, W.M. (Ed.), Encyclopedia of Geochemistry, Encyclopedia of Earth Sciences Series. Springer. https://doi.org/10.1007/978-3-319-39312-4_277.

Rudnick, R.L., Gao, S., 2003. Composition of the continental crust. In: Holland, H.D., Turekian, K.K. (Eds.), The Crust. Elsevier-Pergamon, Oxford, pp. 1–64.

Shaanan, U., Rosenbaum, G., Campbell, M.J., 2019. Detrital fingerprint: the use of early Precambrian zircon age spectra as unique identifiers of Phanerozoic terranes. Earth Planet. Sci. Lett. 506, 97–103. https://doi.org/10.1016/j.epsl.2018.10.039.

Sircombe, K.N., 1999. Tracing provenance through the isotope ages of littoral and sedimentary detrital zircon, eastern Australia. Sediment. Geol. 124, 47–67. https://doi.org/10.1016/S0037-0738(98)00120-1.

Sircombe, K.N., 2004. Age Display: an EXCEL workbook to evaluate and display univariate geochronological data using binned frequency histograms and probability density distributions. Comput. Geosci. 30, 21–31. https://doi.org/10.1016/j.cageo.2003.09.006.

Spencer, C.J., Kirkland, C.L., Taylor, R.J.M., 2016. Strategies towards statistically robust interpretations of in situ U–Pb zircon geochronology. Geosci. Front. 7, 581–589. https://doi.org/10.1016/j.gsf.2015.11.006.

Stacey, J.S., Kramers, J.D., 1975. Approximation of terrestrial lead isotope evolution by a two-stage model. Earth Planet. Sci. Lett. 26, 207–221.

Stampfli, G.M., Borel, G.D., 2002. A plate tectonic model for the Paleozoic and Mesozoic constrained by dynamic plate boundaries and restored synthetic oceanic isochrons. Earth Planet. Sci. Lett. 196, 17–33. https://doi.org/10.1016/S0012-821X(01)00588-X.

Stampfli, G.M., Kozur, H.W., 2006. Europe from the Variscan to the Alpine Cycles. In: Gee, D.G., Stephenson, R.A. (Eds.), European Lithosphere Dynamics. Geological Society of London, p. 0. https://doi.org/10.1144/GSL.MEM.2006.032.01.04.

Staub, R., 1917. Das Äquivalent der Dentblanchedecke in Bünden. Vjschr. Nat. Ges. Zürich 62, 349–370.

Szymanowski, D., Fehr, M.A., Guillong, M., Coble, M.A., Wotzlaw, J.-F., Nasdala, L., Ellis, B.S., Bachmann, O., Schönbächler, M., 2018. Isotope-dilution anchoring of zircon reference materials for accurate Ti-in-zircon thermometry. Chem. Geol. 481, 146–154. https://doi.org/10.1016/j.chemgeo.2018.02.001.

Talavera, C., Montero, P., Martínez Poyatos, D., Williams, I.S., 2012. Ediacaran to Lower Ordovician age for rocks ascribed to the Schist–Graywacke Complex (Iberian Massif, Spain): evidence from detrital zircon SHRIMP U–Pb geochronology. Gondwana Res. 22, 928–942. https://doi.org/10.1016/j.gr.2012.03.008.

Thomas, J.B., Watson, E.B., Spear, F.S., Shemella, P.T., Nayak, S.K., Lanzirotti, A., 2010. TitaniQ under pressure: the effect of pressure and temperature on the solubility of Ti in quartz. Contrib. Mineral. Petrol. 160, 743–759.

Vavra, G., Gebauer, D., Schmid, R., Compston, W., 1996. Multiple zircon growth and recrystallization during polyphase late Carboniferous to Triassic metamorphism in granulites of the Ivrea Zone (Southern Alps): an ion microprobe (SHRIMP) study. Contrib. Mineral. Petrol. 122, 337–358.

Vavra, G., Schmid, R., Gebauer, D., 1999. Internal morphology, habit and U-Th-Pb microanalysis of amphibolite-to-granulite facies zircons: geochronology of the Ivrea Zone (Southern Alps). Contrib. Mineral. Petrol. 134, 380–404.

Vermeesch, P., 2012. On the visualisation of detrital age distributions. Chem. Geol. 312–313, 190–194. https://doi.org/10.1016/j.chemgeo.2012.04.021.

Whitehouse, M.J., Kamber, B.S., 2004. Assigning Dates to Thin Gneissic Veins in High-Grade Metamorphic Terranes: a Cautionary Tale from Akilia, Southwest Greenland. J. Petrol. 46, 291–318. https://doi.org/10.1093/petrology/egh075.

Wiedenbeck, M., Allé, P., Corfu, F., Griffin, W.L., Meier, M., Oberli, F., Quadt, A.V., Roddick, J.C., Spiegel, W., 1995. Three natural zircon standards for U-Th-Pb, Lu-Hf, trace element and REE analyses. Geostand. Newslett. 19, 1–23. https://doi.org/10.1111/j.1751-908X.1995.tb00147.x.

Wiedenbeck, M., Hanchar, J.M., Peck, W.H., Sylvester, P., Valley, J., Whitehouse, M., Kronz, A., Morishita, Y., Nasdala, L., Fiebig, J., Franchi, I., Girard, J.-P., Greenwood, R.C., Hinton, R., Kita, N., Mason, P.R.D., Norman, M., Ogasawara, M., Piccoli, P.M., Rhede, D., Satoh, H., Schulz-Dobrick, B., Skår, O., Spicuzza, M.J., Terada, K., Tindle, A., Togashi, S., Vennemann, T., Xie, Q., Zheng, Y.-F., 2004. Further Characterisation of the 91500 Zircon Crystal. Geostand. Geoanal. Res. 28, 9–39. https://doi.org/10.1111/j.1751-908X.2004.tb01041.x.

Wyatt, D.C., Smye, A.J., Garber, J.M., Hacker, B.R., 2022. Assembly and Tectonic Evolution of Continental lower Crust: Monazite Petrochronology of the Ivrea-Verbano Zone (Val Strona di Omegna). Tectonics 41. https://doi.org/10.1029/2021TC006841 e2021TC006841.

Yakymchuk, C., 2023. Prograde zircon growth in migmatites. J. Metamorph. Geol. 41, 719–743. https://doi.org/10.1111/jmg.12715.

Yakymchuk, C., Brown, M., 2014. Behaviour of zircon and monazite during crustal melting. J. Geol. Soc. 171, 465–479. https://doi.org/10.1144/jgs2013-115.

Zurbriggen, R., 2017. The Cenerian orogeny (early Paleozoic) from the perspective of the Alpine region. Int. J. Earth Sci. 106, 517–529. https://doi.org/10.1007/s00531-016-1438-5.